This is to certify that the

thesis entitled

Geochemical Mass Balance Models of Sandstone Weathering in the Pennsylvanian Recharge Beds of South-Central Michigan

presented by

Jason Rodney Price

has been accepted towards fulfillment
of the requirements for

M.S. degree in Geological Sciences

Michael Anthony Velbel
Major professor

Date 7/8/94

GEOCHEMICAL MASS BALANCE MODELS OF SANDSTONE WEATHERING IN THE PENNSYLVANIAN RECHARGE BEDS OF SOUTH-CENTRAL MICHIGAN

By

Jason Rodney Price

A THESIS

Submitted to
Michigan State University
in partial fulfillment of the requirements
for the degree of

MASTER OF SCIENCE

Department of Geological Sciences

1994

ABSTRACT

GEOCHEMICAL MASS BALANCE MODELS OF SANDSTONE WEATHERING IN THE PENNSYLVANIAN RECHARGE BEDS OF SOUTH-CENTRAL MICHIGAN

By

Jason Rodney Price

Outcrop Pennsylvanian sandstones located near Grand Ledge, Michigan were studied in order to evaluate the chemical and textural effects of weathering. The exposure of these sandstones is the result of post-Pleistocene river down-cutting, and reflect weathering since that time. A comparison is made to subsurface Pennsylvanian sandstones which serve as pre-weathering analogs.

Mass balance calculations suggest that iron is being conserved in the sandstone with the joint block interiors serving as net exporters of iron to the 1 cm thick case-hardened joint faces. All other major cations, including Al^{3+}, are being mobilized from the outcrop through dissolution.

The mass balance calculations for each ionic species are compared with shallow aquifer water chemistry data. This comparison suggests that quartz, carbonates, and pyrite are currently altering in the subsurface. Outcrop K-feldspar appears stable, while muscovite and kaolinite are weathering and the aluminum is being mobilized into the aquifer.

DEDICATION

This thesis is dedicated to a dear friend and mentor, Mr. Richard C. Noreen. Dick's sudden hospitalization in November 1993, and death in December 1993, resulted in the loss of a valued member of the NIU and DeKalb communities. His genuine interest in people, unending willingness to offer a helping hand, and sincere concern for both colleagues and students at Northern Illinois University will long be remembered. Thanks for all the perverted jokes, meals, gifts, and general unselfishness over the years, buddy. You'll never be replaced.

ACKNOWLEDGMENTS

The individual who could not possibly be thanked enough for his help, is my thesis advisor, Dr. Michael Velbel. His humble disposition, cynical sense of humor, and tactful, patient criticisms are tremendously appreciated

Also deserving of recognition are my committee members, Dr. Sibley and Dr. Westjohn. Dr. Sibley always returned no-nonsense answers to my all too often spontaneous questions. Dr. Westjohn provided voluminous material on the subsurface of the Michigan basin, including beautiful thin sections, clay mineral data, and diagenesis research.

A sincere thank you to my parents who empathetically and patiently listened to my stories of frustration, as well as indirectly funding a large portion of my education.

Noteworthy, too, is Tina Beals who was kind enough to perform the silica analyses of my Grand Ledge spring water.

I also cannot forget all of my fellow graduate students who served as both friends and colleagues during my tenure at Michigan State. Kris Huysken, Ditters, Wei Huang, Bill Sitarz, Steve Reigel, Jolene & Bruce Meissner, Cheol Woon Kim, Jaeman Lee, Jon Kolak, and many others too numerous to mention. Thanks folks!

Partial funding for this project was provided by the Michigan Basin Geological Society.

TABLE OF CONTENTS

LIST OF TABLES

LIST OF FIGURES

CHAPTER 1: INTRODUCTION

This investigation examines the weathering of the Upper Pennsylvanian (Conemaugh?) Eaton sandstone (Figure 1) which crops out near Grand Ledge, Michigan (SW 1/4, section 2, T 4 N, R 4 W, Oneida Township, Eaton County) (Figure 2). These outcrops are the result of post-Pleistocene river down-cutting and, therefore, exhibit weathering, much of which is likely post-glacial. These and other Pennsylvanian sandstones in the subsurface of the Michigan basin presently produce fresh-potable waters, with the outcropping and near surface sandstones providing a recharge zone for meteoric water.

Paragenetic sequences and dissolution textures of authigenic minerals in Pennsylvanian sandstone aquifers suggest that basin-wide evolution of a brine produced the authigenic mineral suite prior to post-Pleistocene time (Westjohn et al., 1991; Westjohn & Sibley, 1991). Therefore, the pre-Pleistocene authigenic mineral suite of the Pennsylvanian aquifers in the Michigan basin may be viewed as the pre-weathering mineralogy of the subaerially exposed Eaton sandstone.

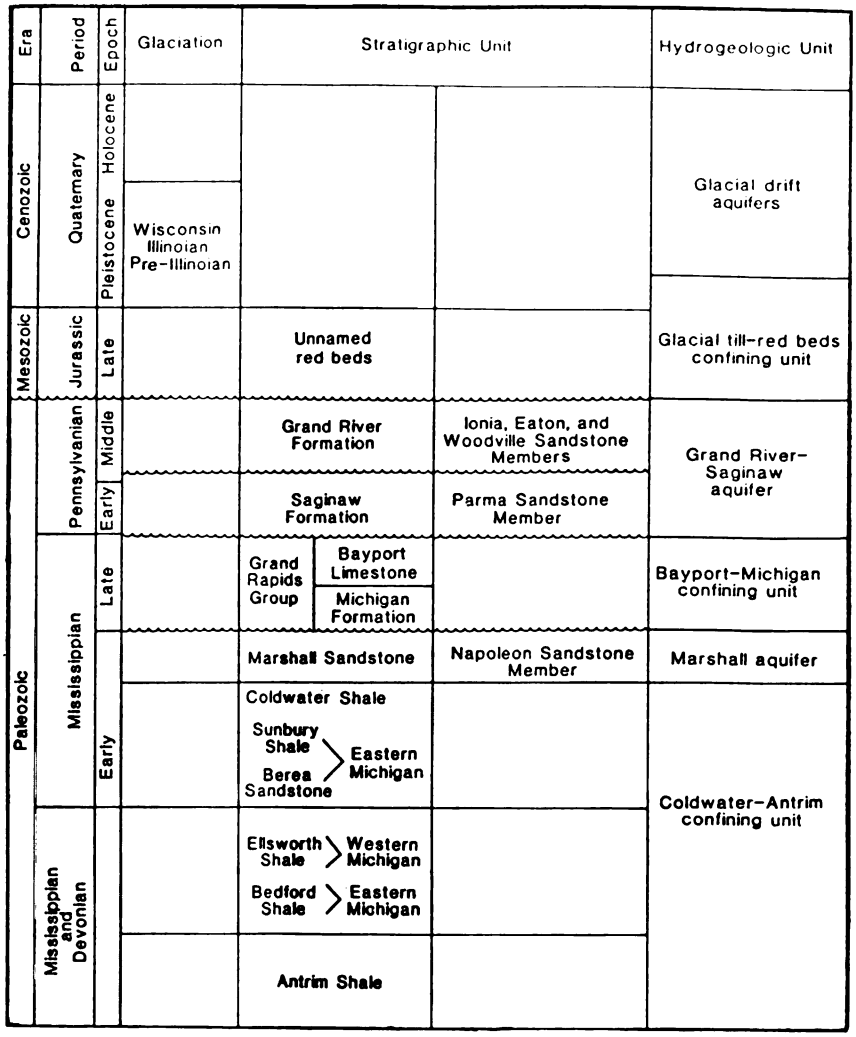

Figure 1. Partial stratigraphic column of the Michigan basin. (From Dannemiller & Baltusis, 1990.)

PURPOSE AND SCOPE

The purpose of this study is to compare the authigenic mineralogy of subaerially exposed Pennsylvanian sandstones with the age-equivalent subsurface rocks found deeper in the Michigan basin (Table 1). Although it has been established that the Pennsylvanian sequence near Grand Ledge is the most extensive natural outcrop of rocks of such age in Michigan (Kelly, 1933), little work has been performed to identify the effects of weathering, and no attempt has been made to relate the authigenic mineralogy of the subsurface age-equivalent rocks to the alteration of the subaerially exposed sandstones.

Outcrop characteristics of sandstones are important in the evaluation of certain categories of potential reservoirs for oil and gas. If correct conclusions on reservoir potentials are to be made, the effects of weathering on the sandstone must be established. Weathered zones exhibit significant secondary porosity which, when trapped below unconformities, may provide potential hydrocarbon reservoirs (Heald et al., 1979; Shanmugam & Higgins, 1988; Shanmugam, 1988, 1990). By comparing the effects of weathering with the pre-weathering mineralogy established from subsurface drill cuttings, this investigation will provide insight into the nature of porosity evolution at unconformities.

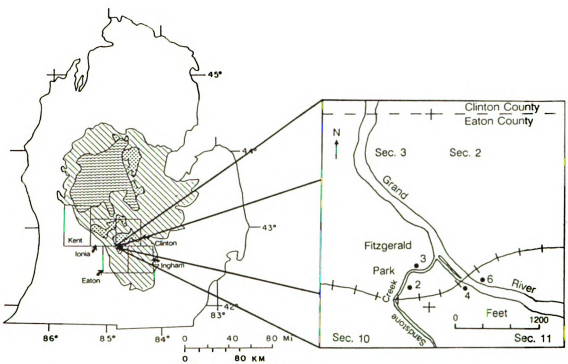

Figure 2. Geology of south-central Michigan and index map of the Grand Ledge area. Dots with numbers represent outcrop sample locations (Appendix B). (Hashed area is Pennsylvanian Saginaw formation, stippled area is Pennsylvanian Grand River formation, and the inverted wave area is Upper Jurassic rocks; modified from Dannemiller and Baltusis, 1990, Figures 1 & 2; and Martin, 1982, Figure 1.)

PREVIOUS WORK

Surficial Geology

Eaton Sandstone

The Eaton sandstone of the Grand River Formation forms the ledges of the Grand River and its tributary, Sandstone Creek, in the northern part of Eaton and southern part of Clinton counties, Michigan (Figure 2). Being the most extensive natural exposure of Pennsylvanian strata in the state of Michigan, the Eaton sandstone provides an important resource for investigations into many aspects of Pennsylvanian geology, including the diagenesis and weathering of Pennsylvanian sandstones. It is a porous, thickly bedded, medium grained, buff-colored quartz arenite to subarkose (Figure 3), having a maximum thickness in outcrop of approximately 18 m (Kelly, 1933; Hudson, 1957; Martin, 1982).

Diagenetic alterations include quartz cement and feldspar alteration (Martin, 1982) (Table 1). Honeycomb weathering is well developed in the Eaton sandstone, and is apparently a function of the presence of salts on the outcrop surface, the aspect of the outcrop, and the massiveness (homogeneity of texture and fabric) of the unit (Wallis & Velbel, 1985). The same researchers also noted the presence of limonite cements forming a well-indurated 1 cm thick zone along joint surfaces. The limonite cement must have formed following sufficient induration of the sandstone to allow brittle deformation. Velbel & Genuise (1988) have studied the non-bedded mudrocks

Table 1. Comparison of subsurface and outcrop mineralogy of Carboniferous sandstones in the Michigan basin.

A. PETROGRAPHIC MINERALOGY

Detrital Mineralogy	Outcrop Pennsylvanian	Subsurface Pennsylvanian	Subsurface Mississippian
Quartz	X[2]	X[6]	X[12]
K-Feldspar	X[2]	X[6]	X[12]
Rock Fragments	X[2]	X[6]	
Muscovite	X[2]	X[6]	X[12]
Chlorite			X[12]

Authigenic Mineralogy	Outcrop Pennsylvanian	Subsurface Pennsylvanian	Subsurface Mississippian
Anhydrite		X[10]	X[10]
Ankerite		X[5,8,10]	X[8,10]
Barite		X[8]	X[8]
Calcite		X[5-10]	X[8-12]
Chlorite		X[6,7,8,10]	X[8-11]
Dolomite		X[5,7,8,10]	X[8,10,12]
Feldspar		X[7,10]	X[10,11]
Glauconite		X[8]	X[8]
Gypsum		X[7,8,10]	X[8,10,12]
Illite	X[13]	X[6,7,10]	X[9,10,11]
Iron Oxy-Hydroxides	X[2](Goethite)[13]	X[7,8,10]	X[8,10,12]
Kaolinite	X[13]	X[6,7,8,10]	X[8-12]
Mixed Clays		X[8]	X[8]
Rhodocrosite		X[5,10]	X[10]
Siderite		X[5,7,10]	X[10]
Quartz	X[1,2,13]	X[8,10,13]	X[8-12]
Witherite		X[5,10]	X[10]
Vermiculite	X[13]		

Table 1. (cont'd).

B. HEAVY MINERALOGY

Detrital Mineralogy	Outcrop Pennsylvanian	Subsurface Pennsylvanian	Subsurface Mississippian
Actinolite			X[12]
Apatite	X[2]		
Biotite			X[12]
Cassiterite	X[1]		
Chlorite			X[12]
Epidote			X[12]
Garnet	X[1]		X[12]
Hornblende			X[12]
Ilmenite			X[12]
Kyanite	X[1]		
Leucoxene			X[12]
Magnetite			X[12]
Monazite	X[1]		
Pyroxene*	X[2]		X[12]
Rutile			X[12]
Staurolite	X[1]		
Tourmaline	X[1,2,4]	X[6]	X[12]
Zircon	X[1,2,4,13]	X[6]	X[12]

*Pyroxene in outcrop is pigeonite, and in the subsurface is enstatite and hypersthene.

Authigenic Mineralogy	Outcrop Pennsylvanian	Subsurface Pennsylvanian	Subsurface Mississippian
Celestite			X[12]
Chlorite		X[6,7,8,10]	X[8-11]
Pyrite		X[6,7,10]	X[10-12]

[1] Hudson, 1957
[2] Martin, 1982
[3] Davis & Bredwell, 1978
[4] Kelly, 1936
[5] Kramer & Westjohn, 1991
[6] Westjohn, written communication
[7] Long et al., 1988
[8] Westjohn et al., 1990
[9] Westjohn & Sibley, 1991
[10] Westjohn et al., 1991
[11] Zacharias, 1992
[12] Stearns, 1933
[13] This study

which occur as lenses in the Eaton sandstone and determined them to consist of kaolinite, illite, lepidocrocite, minor amounts of chlorite, and interstratified illite-vermiculite. The lepidocrocite is believed to be related to local groundwater flow in the Eaton sandstone (Velbel & Brandt, 1989).

Studies of Other Basins

General. Numerous authors have described subaerial diagenesis. Notable among these is Fairbridge (1967) who suggested the term "epidiagenesis" for surficial weathering and the resulting development of new textures and minerals. Al-Gailani (1981) has described the diagenesis of unconformities with emphasis on authigenic mineral formation at paleo-surfaces and the resulting adverse effects on reservoir characteristics. Emery et al. (1990) have used potassium feldspar leaching by meteoric water and kaolinite abundances to demonstrate the presence of burial unconformities. Tardy (1971) and Bjorlykke (1984) have discussed the importance of secondary porosity by describing potassium feldspar dissolution in freshwater and the associated kaolinite precipitation.

Typically, lateral and vertical variations in lithology complicate the study of sandstone weathering by making it difficult to compare weathered and unweathered rock. Furthermore, it is not always clear which secondary alterations are of deep diagenetic origin and which are truly the products of subaerial alteration. In a study of the

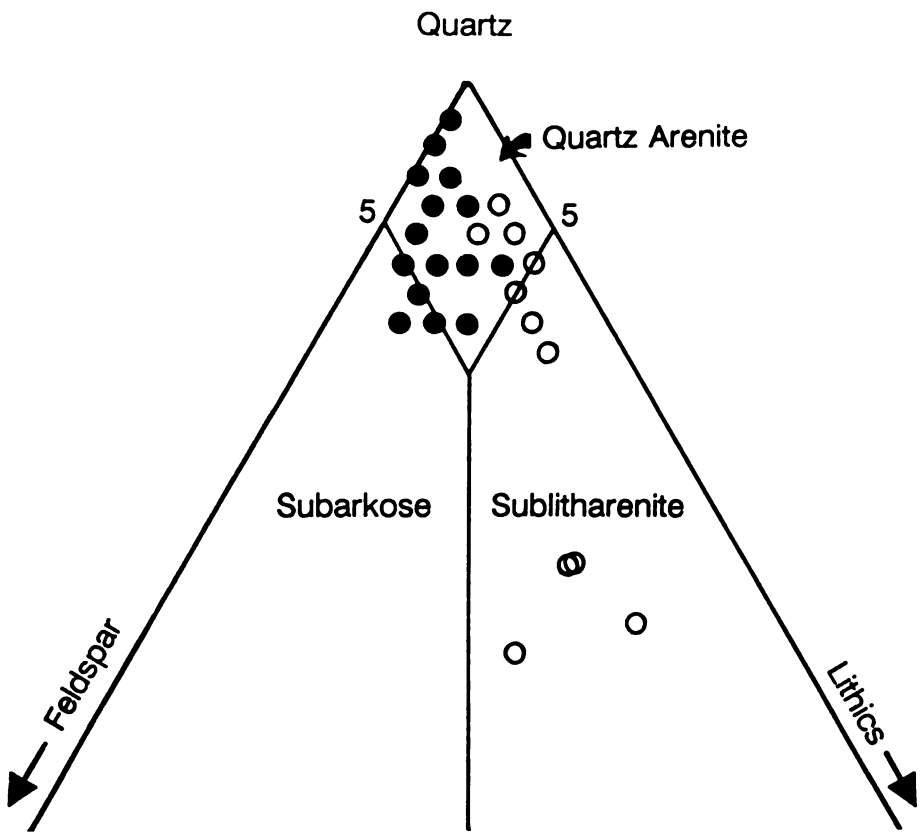

Figure 3. Ternary diagram showing the composition of the Eaton sandstone. Solid circles are outcrop samples and open circles represent subsurface samples. See text for discussion. (Classification of Pettijohn et al., 1987).

spheroidal weathering of the Pennsylvanian Kanawha Formation of central and southern West Virginia, Heald et al. (1979) had great success when comparing the weathered rock to fresh rock cores a short distance away, treating the core mineralogy as pristine and pre-weathering. These researchers believe that an absence of oxidized minerals in outcrop suggests a lack of weathering, and supported this conclusion with subsurface data. In addition, they attributed their outcrop K-feldspar voids to subsurface diagenesis.

Weathering patterns similar to those found in the Eaton sandstone at Grand Ledge, Michigan have been described for the Virgelle Member of the Cretaceous-aged Milk River Formation in Alberta, Canada (Campbell, 1991). This investigator found the sandstone to exhibit alveolar weathering, and thin case-hardened resistant zones of iron-rich varnish, and attributed much of the weathering to ice and salt crystal growth.

Geomorphology. Thiry et al. (1988) and Thiry and Milnes (1991) took a geomorphologic approach to sandstone weathering. These researchers found pedogenic and groundwater silcretes, and attributed their formation to the lowering of the water table during river down-cutting. This work implies that quartz cement does not behave as a seal, and as long as groundwater rises (in the case of early diagenesis), or falls (in the case of subaerial weathering) sufficiently slowly, continuous quartz cementation may proceed as an uninterrupted formation of groundwater silcretes. Furthermore, Thiry et al. (1988) mention that quartz dissolution occurs above the water

table and quartz cementation occurs below the water table. Meissner (1993) found that the waters of the Pennsylvanian aquifers in the Michigan basin are saturated with respect to quartz. As Thiry et al. (1988) have demonstrated for the Paris basin, the Michigan basin exhibits quartz dissolution in outcrop, and quartz saturation below the water table.

Bromley (1992) suggested that the early formation of quartz in the Navajo sandstone of the Colorado Plateau was due to the presence of the unconformably underlying Kayenta mudstone which maintained an elevated groundwater level in the early Navajo sandstone, with evaporation inducing quartz precipitation. However, initial cement accumulation may behave as a seal, preventing further evaporation, and thus cementation (Goudie, 1973; Summerfield, 1983).

Pedogenesis. From a pedogenic perspective glauconitic quartzites have been shown to lateritically weather into "red beds" by glauconitic grains weathering to ferruginous ooids and pisolites in ferricretes (Nahon et al., 1980; Parron & Nahon, 1980).

Vermiculite. Illite may weather to vermiculite (e.g. Adams & Kassim, 1983), but in a study by White (1962), it was demonstrated that the weathering of muscovite produced a 14 Å XRD peak, while the weathered illite peak was simply less intense than the unweathered illite peak. Chittleborough (1989) invokes the opposite weathering reaction, whereby illite weathers from vermiculite.

Ferruginization. Young (1987) reports concentrations of goethite along joint faces of sandstones in the East Kimberley region of Australia, while Nott et al. (1991) found two stages of ferruginization of the Long Beach formation of Australia.

Both pyrite weathering and CO_2 dissolution have been shown to occur in sandstones in a humid region of Japan (Chigira and Sone, 1991), who demonstrated that the formation of iron oxy-hydroxide cement in the oxidation front of the outcrop strengthens the rocks, while beneath this front dissolution of cements weakens the sandstone. Weathering of the pyritic Mahoning sandstone of West Virginia has completely dissolved all pyrite and carbonate, creating sufficiently acidic minesoils to inhibit revegetation (Singh et al., 1982).

Weed & Ackert (1986) report ferruginous oxy-hydroxide precipitation occurring early in their weathering sequence for antarctic sandstones.

Subsurface Geology

Carboniferous Strata of Michigan

Recent work has been conducted on the mineral-water interactions, paragenesis, and diagenesis of the subsurface Pennsylvanian strata of the Michigan basin, as the Grand River Formation is one of the principal bedrock aquifers in the Michigan basin (Westjohn et al., 1990) (Table 1). Westjohn et al. (1990) demonstrated that the cements in the Pennsylvanian sandstones are mineralogically diverse; cements of the poorly to well-cemented sandstones include silica, calcite, ankerite, dolomite, kaolinite, and iron oxide, and lesser amounts of

chlorite, glauconite, barite, mixed-clays, and gypsum cements. Westjohn et al. (1991) observed paragenetic sequences which are the same for both Mississippian and Pennsylvanian sandstones from the Michigan basin, and suggested that the identical authigenic minerals found in these sandstone aquifers are the product of pre-Pleistocene basin-wide chemical evolution of groundwater in Carboniferous strata. A paragenetic sequence for the Marshall sandstone (Mississippian) as determined by Stearns (1933) has quartz precipitation, with calcite filling the interstices between sand grains, followed by pyrite, magnetite (possibly marcasite), and small amounts of celestite. Westjohn & Sibley (1991) state that there is no evidence that flushing with meteoric water during or since the Pleistocene has altered Mississippian clastic sediment authigenic minerals. Studies by Zacharias (1992) and Zacharias et al. (1992) on Mississippian strata in the Michigan basin interpret isotopic data and mineral paragenesis and suggest that cements (chlorite, carbonate, and kaolinite) did not form in equilibrium with present-day pore-fluids. Furthermore, the illite distribution throughout the unit suggests that it may have formed prior to the differentiation of modern-day interstitial fluids (Zacharias, 1992; Zacharias et al., 1992). Since kaolinite is the final phase (Westjohn et al., 1990; Zacharias, 1992) of the paragenetic sequence, and it is not in isotopic equilibrium with modern-day interstitial fluids, it follows that phases precipitated prior to kaolinite are also

not in equilibrium with present-day pore fluids.

Long et. al. (1990) use major element geochemistry and isotopic chemistry of water from deep formations, near surface bedrock, and glacial drift to suggest that any water-rock interaction presently occurs only in the glacial drift. The interacting water is characterized by high salinities, which are believed to be the result of long residence times of the groundwater, thus allowing time for upward diffusion/advection of formation brine into glacial-lacustrine clay. Meissner et al. (1992) inferred that dissolved solids in the Mississippian Marshall sandstone subcrop originated from meteoric water-rock interactions in overlying glacial drift. These same researchers suggest that the evolution of ground water in Mississippian aquifers by dilution of marine brine with meteoric water occurred following geochemical processes such as clay interaction and sulfate reduction, and that this ground water evolution is very similar to that of the underlying Devonian formations. Wahrer et al. (1992) studied ground water in glacial-drift and near-surface-bedrock aquifers and found that the ground water in the latter is at or near equilibrium with respect to calcite, and possibly dolomite.

Studies of Other Basins

General. Bjorkum & Gjilsvik (1988) have described the disagreement regarding open vs. closed systems for authigenic mineral growth and propose an isochemical model for authigenic kaolinite, potassium feldspar, and illite formation. These

authors point out that in an isochemical system, kaolinite may form by the degradation of mica or potassium feldspar, and the a_{K+}/a_{H+} ratio of the pore water will increase and the reaction will reach equilibrium unless either a K^+ sink or, a H^+ source exists. For the Carboniferous sandstones in the Illinois basin, Nesbitt (1980) has suggested that subsurface sodium ions are incorporated in clay minerals rather than bonding to weak neutral complexes in shales.

Ferruginization. McBride (1987) provides a case history of the diagenesis of a subarkose sandstone which, like the Eaton sandstone, contains limonite cement, displays upward-fining of grain size, is a fluvio-deltaic deposit, is well sorted and rounded, and bioturbated. In addition, four plausible diagenetic pathways are presented, with final uplift and weathering resulting in the oxidation of siderite to limonite, goethite, and hematite, as well as the dissolution of calcite producing porosities of up to 20%. Arditto (1983) conducted a study on the mineral-water interactions of the intake beds of the Great Australian (Artesian) basin, and determined that weathering of subsurface siderite cement explains the development of secondary limonite and goethite over the outcrop exposure. Furthermore, the same researcher noted lateral anisotropy with respect to authigenic kaolinite in both outcrop and in the subsurface, and found very porous, water-saturated zones which are generally coated with red-brown iron-oxides. Arditto (1983) believes the more porous zones represent either primary porosity or secondary porosity

by the leaching of carbonate-cemented zones.

Quartz dissolution. A study by Morris and Fletcher (1987) found that redox reactions involving iron result in a much more rapid dissolution of quartz than would be predicted from the known solubility of quartz in water. These researchers conclude that in a ferrous iron solution a single-layer ferrous iron/silica complex forms on the quartz grain surface; this layer breaks down under oxidizing conditions, resulting in a rapid release of silica to solution. In essence, an absence of oxidized minerals suggests a lack of weathering.

HYPOTHESIS

The hypothesis tested here is that subaerial exposure of the Pennsylvanian Eaton sandstone has produced an authigenic mineralogy that can be explained in terms of an open chemical system (allochemical) with a high freshwater flux. This is in contrast to the differing authigenic mineralogy of the subsurface age-equivalent rocks found deeper in the Michigan basin, which may be explained in terms of a closed chemical system (isochemical) with a low water flux. Since the surficial sandstone outcrops are exposed to precipitation, it is expected that ions produced by the degradation of minerals will be transported out of the system.

If appreciable weathering of the Eaton sandstone has occurred, the alteration should be evident in thin section.

Weathering textures may include quartz grains and quartz overgrowths displaying corrosion textures, dissolved calcite, and leached feldspar with concomitant kaolinite. Since illite has been found in the subsurface (Table 1) it may be found weathering to kaolinite or ferruginous oxy-hydroxides, or may be leached away completely. In general, weathering tends to decrease the amount of Si, K, and Mg present, while increasing the quantities of Al and Fe, and producing oxides and hydroxides.

CHAPTER 2: PETROGRAPHY

SAMPLE COLLECTION

Sampling was performed at 4 different locations in the vicinity of Grand Ledge, Michigan (Figure 2, Appendix C). Additional thin sections from a previous worker were also used. At each of the 4 locations 4 to 6 samples were taken starting at the joint face and working toward the interior of the joint block. The orientation of the joint plane, aspect of the outcrop, trend of sampling line, and distance from the joint face that each sample was taken was recorded (Appendix B).

The subsurface thin sections were provided by the U.S. Geological Survey, Lansing, Michigan. All samples with a sample name starting with "B" are from wells drilled in the Bunkerhill area, Ingham County; all those samples starting with an "S" are from the Standish area, Arenac County.

METHODS

Thin sections observed in this study (43 total) were impregnated with blue epoxy. The sandstones were first impregnated, then cut, with the cut side of the billet being

adhered to the slide, so that any plucking of framework grains would create an isotropic hole in the epoxy and be readily distinguishable by the petrographer.

Petrographic evaluation and point counting of the sandstones was performed on a Nikon Labophot-Pol microscope. A mechanical stage was used to advance the thin section and to record the coordinates of noteworthy features. A grid reticule was inserted into the right ocular for the purpose of making petrographic measurements and point counting.

PETROGRAPHIC DESCRIPTION AND INTERPRETATION

The suite of thin sections exhibits extremely little variability. The sandstones are typically very porous (averaging 22.9%, Table 2), with mild alteration of detrital phases, patches of clay, quartz cement, sparse detrital zircon, and limonite coatings on all of the above. The regions of highest porosity are often devoid of limonite coatings, and in these areas detrital grains are commonly rounded (Figure 4a), as opposed to less porous areas of grain angularity (Figure 5a-b). Quartz dissolution features are manifested in thin section and under the SEM as corroded quartz overgrowths (Figures 5 & 6). Point count data indicate an average of 1.8% of quartz dissolution has occurred. All phases, including clay, exhibit dissolution features at some location, although limonite may be found coating dissolution features in detrital and authigenic phases. Dissolution

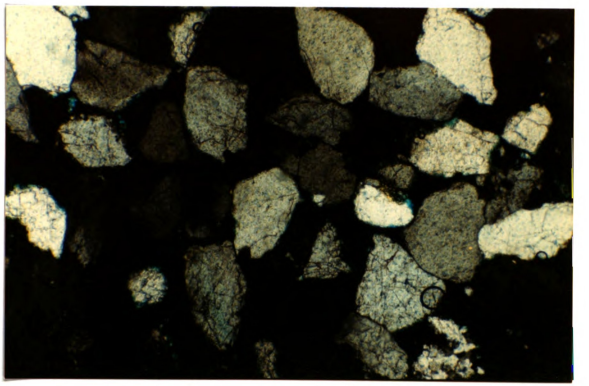

Figure 4. (a) Photomicrograph of the quartzose Eaton sandstone. Notice region devoid of goethite (limonite), and associated grain roundness. Sample JP-95-21. Crossed-polars; field of view is 1.5 mm across.

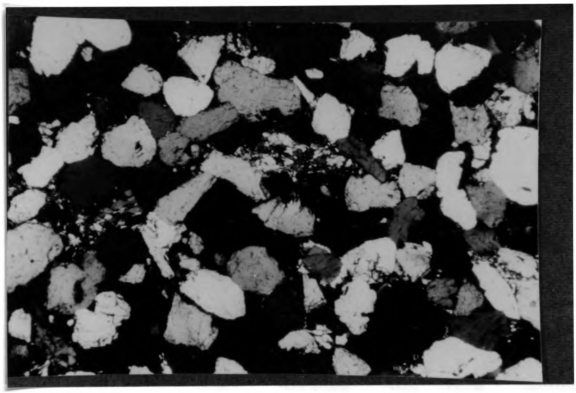

Figure 4. (b) Photomicrograph of a subsurface Upper Pennsylvanian sandstone. Notice similar grain rounding as in (a), as well as carbonate and quartz cements. U.S.G.S. sample J3-81. Crossed-polars; field of view is 2.9 mm across. (Photo courtesy of U.S. Geological Survey, Lansing, Michigan).

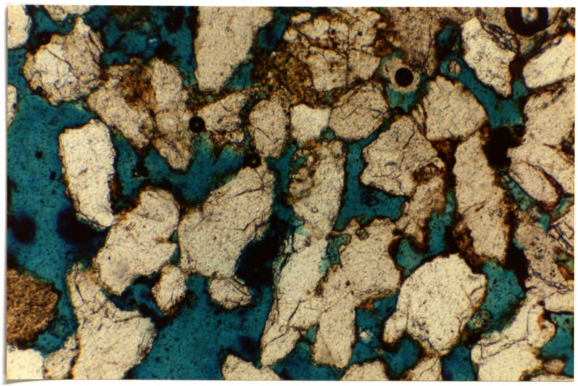

Figure 5. (a) Photomicrograph of the typical Eaton sandstone. Notice goethite (dark brown material), high porosity, microcline, and grain angularity. Sample JP-95-1. Plane-polarized light; field of view is 1.5 mm across.

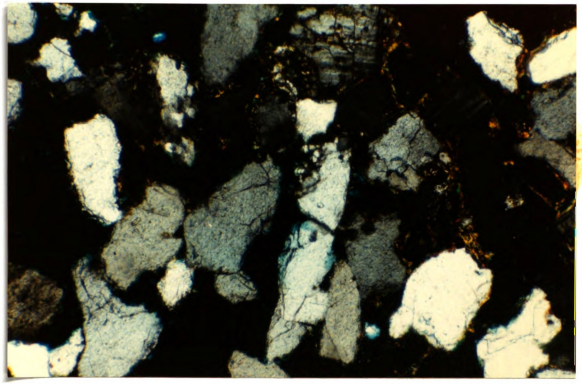

Figure 5. (b) Same view as in (a) but under crossed-polars. Goethite is birefringent orange material.

Table 2. Outcrop Pennsylvanian sandstone modal mineralogies.

Sample	Inches from joint	Quartz	Porosity	Carbon.	K-Spar	Kaolin.	Musc.	Pyrite	Lithics	Goethite	▲Other
JP-95-1A	0.00	61.5	6.6	0	2.9	1.2	0	0	2.2	19.2	1.0
JP-95-1B	0.75	61.5	25.8	0	2.9	1.2	0	0	2.2	5.4	1.0
JP-95-2	2.75	67.6	21.5	0	3.4	1.7	0.3	0	0.8	4.2	0.6
JP-95-3	5.25	64.8	20.3	0	2.6	1.0	0	0	1.3	8.9	1.1
JP-95-4	7.50	68.8	23.6	0	1.8	1.0	0	0	1.5	2.0	1.5
JP-95-5	10.00	60.0	31.0	0	3.6	1.0	0	0	1.9	2.4	0.2
JP-95-6	13.25	64.2	25.8	0	3.1	1.4	0	0	1.1	2.5	1.9
JP-95-7A	0.00	56.7	5.3	0	3.7	0.0	0	0	1.0	21.3	0.7
JP-95-7B	0.75	56.7	5.3	0	3.7	0.0	0	0	1.0	11.3	0.7
JP-95-8	3.00	67.0	16.2	0	1.7	0.3	0	0	0.8	13.7	0.3
JP-95-9	5.25	58.5	25.0	0	1.2	0.2	0.2	0	0.5	14.4	0.0
JP-95-10	7.50	64.1	18.4	0	1.1	0	0	0	2.5	13.3	0.6
JP-95-11	9.75	61.9	24.9	0	3.5	0	0	0	0.8	7.5	1.3
JP-95-12A	0.00	59.7	12.1	0	1.3	0.5	0	0	1.1	20.0	0.8
JP-95-12B	0.75	59.7	32.1	0	1.3	0.5	0	0	1.1	4.5	0.8
JP-95-13	3.13	66.4	24.4	0	1.5	0.6	0	0	0.9	5.9	0.3
JP-95-14	5.25	65.4	20.4	0	1.4	1.4	0	0	0.3	10.6	0.6
JP-95-15	7.38	69.1	19.7	0	1.4	1.4	0	0	1.4	6.6	0.3
JP-95-16A	0.00	66.8	4.7	0	1.4	0.6	0	0	0.9	18.4	0.3
JP-95-16B	1.00	66.8	23.1	0	1.4	0.6	0	0	0.9	6.9	0.3
JP-95-17	3.75	64.7	19.4	0	1.2	2.6	0.6	0	2.6	8.1	0.9
JP-95-18	6.00	64.4	26.2	0	2.7	0.8	0.5	0	1.6	3.5	0.3
JP-95-19	8.25	64.5	24.9	0	2.6	0.3	0.3	0	0.6	6.3	0.6
JP-95-20	10.75	73.6	17.4	0	1.0	0.7	0	0	0	7.0	0.3
JP-95-21	13.00	66.4	29.2	0	2.1	0.6	0.3	0	0	1.2	0.3
JP-95-22	--	73.2	20.0	0	0.6	1.3	0	0	2.3	2.6	0.0
JW-1-3	--	69.1	20.1	0	1.5	1.2	0	0	1.2	5.8	1.2
JW-3-4	--	68.7	18.9	0	0.8	0.8	0.8	0	2.2	7.5	0.3
JW-1-1	--	74.6	20.5	0	1.6	0.6	0	0	1.6	0	1.0
JW-13-2	--	74.8	21.5	0	1.9	0.3	0	0	0.9	0	0.6
JW-24-6	--	69.1	22.2	0	2.1	0.3	0	0	0.6	5.7	0.0
JW6-3(6)	--	61.1	26.1	0	1.6	1.1	0	0	2.6	3.5	4.0
JW-5-8	--	68.7	18.1	0	1.6	0.8	0.8	0	2.1	7.6	0.3
JW-E-1-3	--	64.3	26.5	0	1.7	0.6	0	0	1.1	5.0	0.8
JW-23	--	67.5	25.5	0	2.0	0.8	0.8	0	0.3	2.8	0.3
JW-25	--	65.1	24.4	0	1.4	0.3	0	0	0	8.6	0.3
JW-8(10)	--	72.1	18.7	0	2.1	1.8	0.3	0	1.2	1.8	2.1
JW-0(11)	--	73.9	15.4	0	1.6	0	0	0	1.0	8.0	0.0
JW-17-8	--	61.2	25.0	0	3.2	0.6	0.2	0	1.4	8.0	0.4
JW-8(13)	--	72.5	20.1	0	2.2	0.6	0.3	0	1.0	2.9	0.3
JW-19(14)	--	68.5	14.1	0	0.6	0	0	0	0	16.2	0.6
JW12-17-3	--	66.7	18.8	0	1.1	0.3	0	0	0.3	12.8	0.0
JW12-17-4	--	65.6	26.2	0	1.3	1.2	0.2	0	2.5	3.0	0.0
JW12-17-5	--	64.5	26.1	0	2.7	0.8	0.5	0	1.7	3.4	0.3
JW-11-5	--	58.9	30.1	0	1.3	0.6	0	0	0.9	7.9	0.3
JW-14-2	--	61.1	25.9	0	1.5	1.1	0	0	2.4	4.3	3.7
JW-11-2	--	56.7	26.0	0	3.1	0.3	0	0	1.8	11.0	1.1
Mean		65.9	22.9	0	2.0	0.7	0.1	0	1.2	6.4	
Standard Dev.		4.8	4.2	0	0.8	0.6	0.2	0	0.8	4.0	
Minimum		56.7	14.1	0	0.6	0	0	0	0	0	
Maximum		74.8	32.1	0	3.7	2.6	0.8	0	2	21.3	

▲"Other" refers to plucked grains, zircons, or unidentifiable material.

features are manifested as jagged edges bounding a pore. Those samples collected from outcrop #3 (Figure 2) contain far more limonite than any other outcrop.

Quartz

Description

Quartz comprises 56-75% of the framework grains (Table 2). Intergrown boundaries with quartz cement are common, but dust rims are extremely scarce, suggesting very early quartz cementation. The persistence of well-rounded argillaceous rock fragments suggests a lack of compaction which may be the result of early quartz cementation at a shallow depth. The reader is referred to page 10 for a discussion of shallow quartz cementation.

Some quartz grains exhibit a maroon oxy-hydroxide fracture filling which petrographically appears to be inherited from the source region since it does not extend beyond the limits of the host quartz grain. Also observed was what appears to be quartz replacement by clay. This replacement manifests itself as small yellow clay flakes being inserted into the outer edge of the quartz grain. In the subsurface it was verified that illite was replacing quartz using EDS on Upper Pennsylvanian sandstones (Westjohn, written communication). XRD data on the overlying Eaton sandstone of this study confirms the presence of illite (Table 5). Isolated vermicular molds are also present, and are sometimes limonite filled in a few detrital quartz grains (Figure 15). This iron-bearing vermicular clay was either inherited from

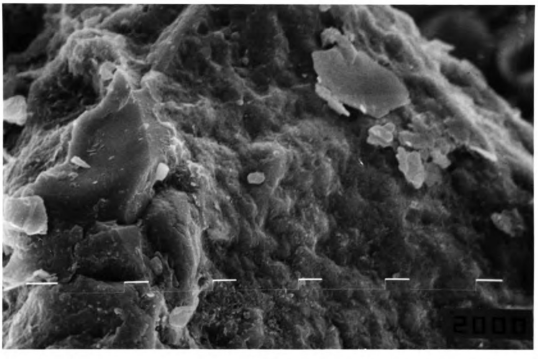

Figure 6. Scanning electron micrograph of weathered quartz showing corrosion of quartz over-growths. Sample JP-95-17. Bold bars are 10 μm apart.

the source region or formed diagenetically; it will be seen later in this thesis that the mineral is chlorite.

The Role of Ferruginization in Quartz Solubility

As stated above, quartz grains are angular in areas where porosity has been partially occluded by limonite, while sub-rounded to rounded in areas of greatest porosity and limonite is absent. The lack of limonite is likely a result of the higher iron mobility due to the higher rate of the meteoric pore-water flow. Nedkvitne & Bjorlykke (1992) use the same theory, with aluminum however, to explain an absence of kaolinite in facies of high secondary porosity. This may suggest that the limonite is responsible for quartz dissolution. It is questionable whether quartz dissolution is associated with the precipitation or dissolution of neoformed limonite. The observation that limonite fills dissolution cavities and fractures implies that dissolution of quartz occurred prior to the precipitation of limonite. However, it is generally believed that quartz is only soluble in alkaline waters (e.g Krauskopf, 1956; Siever, 1962), and the precipitation of limonite releases protons, which would produce acidic conditions. It is possible, therefore, that the dissolution of limonite (an hydrogen consuming reaction) may provide an alkaline microenvironment suitable for quartz dissolution. Limonite dissolution is exhibited in thin section by the presence of limonite in dissolution cavities, while being absent on the outermost edges of the quartz grain. For alkaline meteoric pore-water to reach the quartz surface,

it must infiltrate the limonite surface layer. If this had occurred, then a dissolution void would exist between the quartz and limonite; a feature not observed. This discussion leads the author to believe that quartz dissolution is associated with limonite precipitation and not dissolution. The reader is referred to page 16 for a discussion of quartz dissolution.

Quartz Dissolution and pH

Several studies have demonstrated that quartz grain etching may occur in acidic to near neutral-pH environments, in the presence of high dissolved organic carbon concentrations (i.e. Young, 1987, 1988; Bennett & Siegel, 1987; Bennett et al., 1988; 1991). These studies suggest that organic-acid-silica complexes increase quartz solubility and dissolution rates at near neutral-pH environments. However, even though lush vegetation covers most horizontal rock surfaces at Grand Ledge, only thin (<1 m) soils cover the sandstones. Furthermore, a pH measurement of spring water draining the ledges in the Spring of 1994 indicates a pH of 8.8. The high pH is attributed to the dissolution of limonite, but that hypothesis has not been confirmed. The silica concentrations in the spring water is 5.6 mg/l (Beals, personal communication) which indicates silicate mineral dissolution (dominated by quartz) is occurring at present, but is not exceeding equilibrium concentrations, regardless of the high pH (Krauskopf, 1956; Siever, 1962). In addition, at the onset of weathering quartz dissolution was the result of

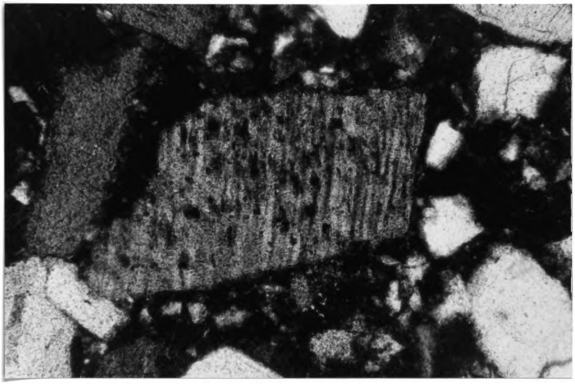

Figure 7. Photomicrograph of a diagenetically altered K-feldspar with etch pits. K-feldspar appears stable in outcrop. Sample JP-95-5. Crossed-polars; field of view is 0.6 mm across.

goethite precipitation, but today quartz dissolution is simply the result of dilute meteoric water reaching equilibrium with respect to silica.

K-Feldspar

Description

K-feldspar composes <1-2% of the framework grains (Table 2), is often fractured, altered along cleavage, and/or exhibiting etch pits (Figure 7). Limonite may or may not be found filling these features. Microcline may be found very pristine.

Muscovite

Description

Although muscovite accounts for less than 1% of the rock, it is still a common, and important, constituent. It may be found conforming around more competent framework grains, as well as exhibiting no indication of compaction (Figure 8a,c). It may also be observed showing signs of dissolution (Figure 8c). Tables 2 & 3 show an average muscovite loss due to dissolution of about 0.3%. SEM photomicrographs (Figure 8b) show muscovite undergoing exfoliation as a result of weathering. Energy Dispersive Spectroscopy (EDS) indicates a potassium depletion in the exfoliating layers relative to the unweathered muscovite. Vermiculite was found to be present in the clay-sized fraction of the sandstone (Table 5), and was not identified in the subsurface (Table 6), and is, therefore, a true weathering product.

Interpretation

The author believes that muscovite is parental to vermiculite based on several lines of evidence (for a complete discussion on vermiculite, the reader is referred to page 11). Chlorite appears in such small quantities in the subsurface (Table 6; words such as "hint," "trace," and "minor" are used to describe chlorite abundances), that it is unlikely that it could result in a vermiculite peak like that observed on the XRD pattern for the outcrop (Appendix A). The above discussion (as well as the discussion found on page 11) implies that muscovite is a more likely vermiculite parent than illite. The alteration of muscovite to dioctahedral vermiculite is well established (e.g. Rich, 1958), who states that the widespread occurrence of dioctahedral vermiculite suggests that the formation of this mineral from muscovite is common. Furthermore, both Rich (1958) and Lin and Clemency (1981) describe the removal of K^+ from the interlayer sites of muscovite with the destruction of the tetrahedral sheets (Si-O bonds) being the rate-controlling mechanism of muscovite dissolution. The removal of the K^+ allows the structure to expand to 14 Å. As stated earlier, potassium depletion was observed in the exfoliating layers of an Eaton sandstone muscovite.

Clay Minerals

Clays occur as patches of mixed yellow-orange, and gray vermicular clays (Figure 9), and often as products of *in situ* weathering of detrital muscovite (Figure 8). The lack of

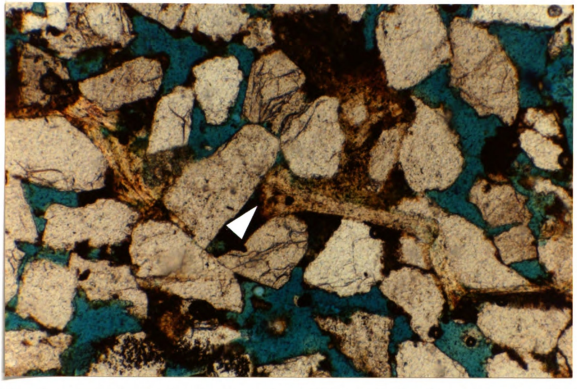

Figure 8. (a) Photomicrograph of altering muscovite showing compaction features and alteration to vermiculite (arrow). Sample JP-95-1. Plane-polarized light; field of view is 1.5 mm across.

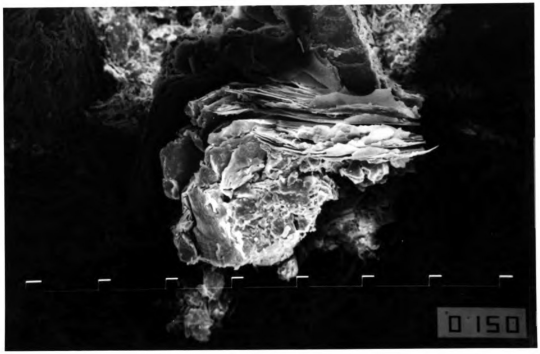

Figure 8. (b) Scanning electron micrograph of parental muscovite with exfoliating vermiculite layers. Sample JP-95-1. Bold bars are 100 μm apart.

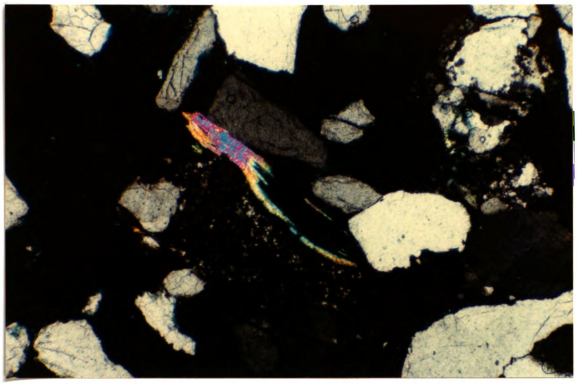

Figure 8. (c) Photomicrograph showing evidence of muscovite dissolution. Sample JP-95-12. Crossed-polars; field of view is 1.5 mm across.

compaction, and presence and persistence of spherical pelitic rock fragments, suggests that any clay present formed post-depositionally, and is not squashed argillaceous rock fragments. Clay loss due to weathering is observed in the Eaton sandstone (Figure 10), and is very important in weakening the sandstone, since the increased porosity may make the rock more sensitive to frost action (Vicente, 1983) or salt wedging. XRD data indicates the presence of abundant, well crystallized kaolinite, and lesser amounts of illite and vermiculite (Table 5; Appendix A). The delicate vermicular crystals of kaolinite suggest a diagenetic origin (Wilson and Pittman, 1977). Reports have been made of vermicular molds in the limonite-rich case-hardened joint faces (Wallis, unpublished data), however, a vermicular kaolinite was found in the joint face using the SEM (Figure 11). The mixed clay patches appear to be preserved where largely enclosed by surrounding framework grains. Clay bounded by relatively large pores typically exhibit dissolution features, and may be coated with limonite. Clay is never found optically continuous with the detrital grains it surrounds, and kaolinite is rarely found associated with microcline.

Pyrite

Three 0.01 mm cubic euhedral opaque grains were also observed (Figure 12). Based on subsurface petrography (Westjohn, written communication) it is believed that these grains are pyrite. Since the pyrite occurs amidst a patch of brown limonitic matrix, no red haloes were observable

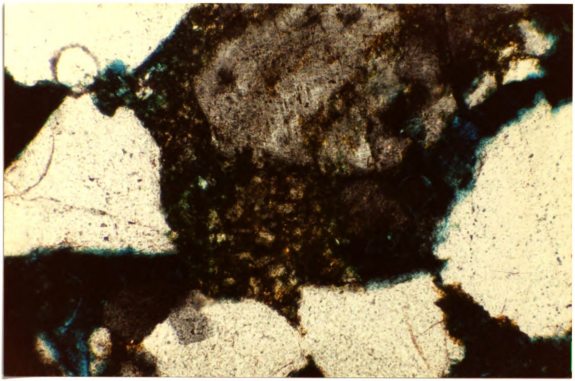

Figure 9. Photomicrograph of a typical diagenetic clay patch. Composition is predominantly kaolinite with lesser illite. Sample JP-95-2. Crossed-polars; field of view is 0.6 mm across.

surrounding them. The euhedral shape of these limonite enclosed pyrite grains suggests that they have not experienced any subaerial weathering, likely due to the protective coating of the limonite.

Ferruginous Oxy-Hydroxides

Description

The presence of limonite (goethite) is characteristic of the outcrop samples. Although most abundant in the 1 cm thick case-hardened joint faces (Figure 16), the goethite also forms the 1-5 mm weathering skins found on the outcrop surface. These skins may penetrate as deep as 3-4 cm in the most heavily weathered outcrop #3 (Figure 2), and are the result of iron being mobilized and reprecipitated at the outcrop face in response to evaporation (Williams & Robinson, 1989). Qualitative XRD results show the presence of goethite, and an absence of detectable hematite in the sandstones. The neoformed goethite typically coats all phases in the rock, including dissolution cavity fillings, fracture fillings, dissolution features in detrital and authigenic minerals, as well as penetrating into the clay patches. Wallis & Velbel (1985) noted the presence of vermicular molds in the limonite at the 1 cm case-hardened joint face, however this study found a goethite covered vermicular kaolinite in the joint face (Figure 11).

Interpretation

Extensive iron staining at springs suggests water draining the outcrop is saturated with respect to the iron

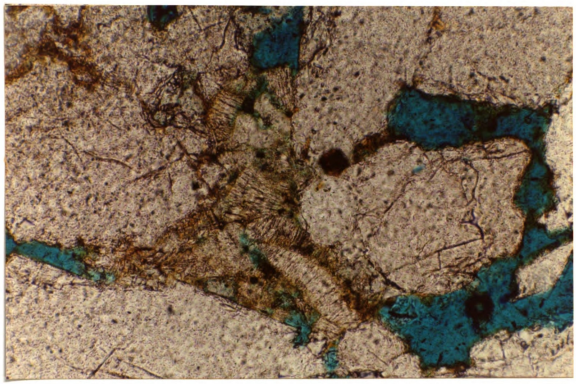

Figure 10. (a) Photomicrograph displaying evidence of kaolinite dissolution. Sample JP-95-1. Plane-polarized light; field of view is 0.6 mm across.

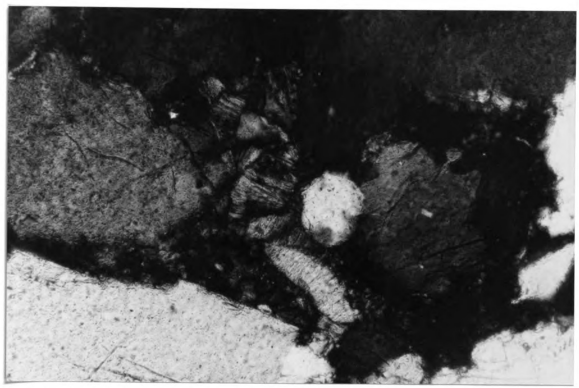

Figure 10. (b) Same view as in (a) but under crossed-polars.

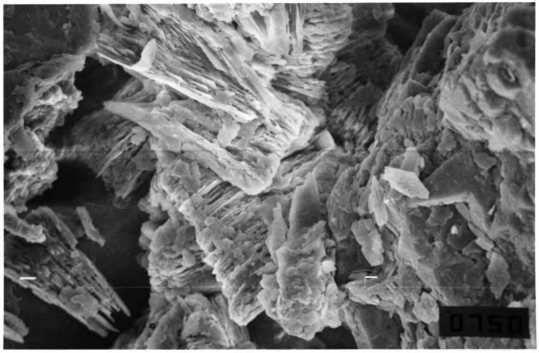

Figure 10. (c) Scanning electron micrograph displaying evidence of kaolinite dissolution. Sample JP-95-21. Bold bars are 100 μm apart.

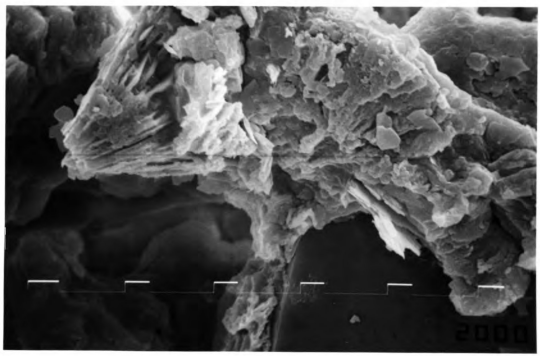

Figure 10. (d) Scanning electron micrograph displaying evidence of kaolinite dissolution. Sample JP-95-10. Bold bars are 10 μm apart.

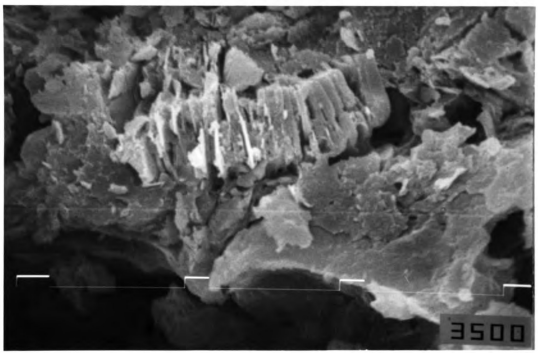

Figure 11. Scanning electron micrograph of a vermicular kaolinite in the 1 cm case-hardened joint face. Wallis (unpublished data) reported finding "vermicular molds" in goethite in the joint face. Sample JP-95-7. Bold bars are 10 μm apart.

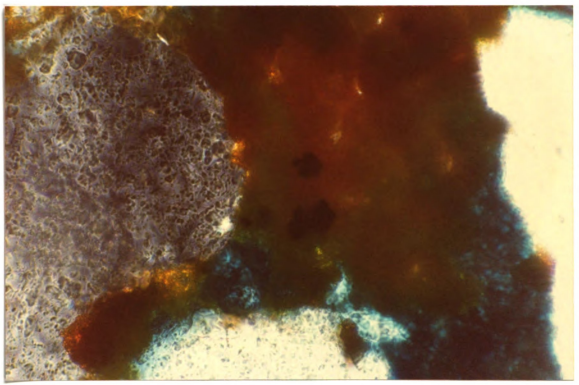

Figure 12. Photomicrograph of what is believed to be pyrite crystals. The crystals appear to be protected from meteoric pore-water by a thick layer of goethite. Sample JP-95-7. Crossed-polars; field of view is 0.24 mm across.

mineral that makes up the stain. This iron is the result of goethite dissolution. Hollingsworth (1977) determined that localized iron oxidation alone was not responsible for changes in outcrop coloration of the Pennsylvanian Kanawha Group in West Virginia. The same author believes that additional iron was introduced *via* groundwater and deposited as an iron hydroxide.

COMPARISON WITH SUBSURFACE PETROGRAPHY

Subsurface petrography is extracted from photomicrographs (Figures 13, 14, & 15) and other researchers' notes (Westjohn, written communication), as well as from the author's own point counts and petrographic observations. A qualitative comparison of subsurface/outcrop mineralogy is provided in Table 1.

Table 3. Subsurface Pennsylvanian sandstone modal mineralogies.

Sample	Quartz	Porosity	Carbon.	Por.+ Carbon.	K-spar	Kaolin.	Musc.	Pyrite	Lithics	▲Other
B2-76	61.9	17.0	4.0	21.0	3.8	3.5	0.3	0	8.3	1.3
B2-80	61.2	12.0	5.1	17.1	4.0	1.1	1.7	0	10.0	4.3
B2-85	66.8	14.3	2.3	16.6	4.3	1.4	1.1	0	8.3	1.4
B2-92	59.9	14.0	8.0	22.0	2.8	2.1	0	0	10.1	2.1
S20-45	69.2	18.7	3.8	22.5	1.3	0.8	0	0	5.7	0.6
S2-47	69.7	18.4	0.3	18.7	0.6	3.1	0	0	2.0	0.3
S13-51	67.9	18.7	8.4	27.1	0.6	0.6	0	0	3.8	0.0
S3-41	66.0	18.4	8.6	27.0	1.2	0.3	0.3	0	4.9	0.3
S3-118	66.2	15.8	9.9	25.7	1.6	0.6	0.6	0	3.4	1.2
S3-65.5	78.1	10.4	4.7	15.1	1.3	0.7	0	0	2.7	1.0
S3-109.5	74.2	17.5	3.1	20.6	0.6	0.6	0.3	0	3.4	0.0
S3-134	71.1	19.0	2.3	21.3	1.4	0	0.3	0	5.1	0.9
Mean	67.7	16.2	5.0	21.1	2.0	1.2	0.4	0	5.6	
Std. Dev.	7.0	5.3	3.0	3.96	1.4	1.1	0.5	0	2.9	
Minimum	59.9	10.4	0.3	15.1	0.6	0.0	0.0	0	2.0	
Maximum	78.1	19.0	9.9	27.1	4.3	3.5	1.7	0	10.1	

▲"Other" refers to plucked grains, zircons, or unidentifiable material.

Carbonate

Carbonate phases compose the most abundant cement in the subsurface (Figure 13). Point count data from these sandstones shows modal carbonate ranges of 0-10%, but in several samples where carbonate is recorded as occurring in trace abundances it is noted that the carbonate "looks as though it was extensive, mostly dissolved," (Westjohn, written communication). If carbonate and porosity values are combined, values of 15-27% are obtained, averaging 21% (Table 3). Subsurface carbonate dissolution is reported to be producing iron oxide (Table 4), carbonate being a source for the goethite found in outcrop (Figure 14). Numerous researchers have reported a diagenetic siderite source of epidiagenetic iron oxy-hydroxides (e.g. Heald et al., 1979; Arnold, 1978; Hollingsworth, 1977; Arditto, 1983; Young & Young, 1988).

Table 4. Report on carbonate abundances in subsurface thin sections. (Westjohn, written communication.)

Carbonate	Subsurface Report
Siderite	Forms abundant "concretions." Reported altering to iron oxide, and filling fractures.
Ankerite	Patchy carbonate cement in "S" and "B" suites is ankerite. Initially "...constitutes a majority of observed carbonates."
Dolomite	Ankerite zones to dolomite on edges. "Dolomite is rare..."
Calcite	Samples with all carbonates present only have "...rare calcite..." which is "...almost exclusively poikiloblastic..."

Figure 13. (a) Photomicrograph of subsurface "pre-weathering" carbonates displaying both poikilitic carbonate and rhombs. U.S.G.S. sample B2-92. Crossed-polars; field of view is 2.9 mm across. (Photo courtesy of U.S. Geological Survey, Lansing, Michigan).

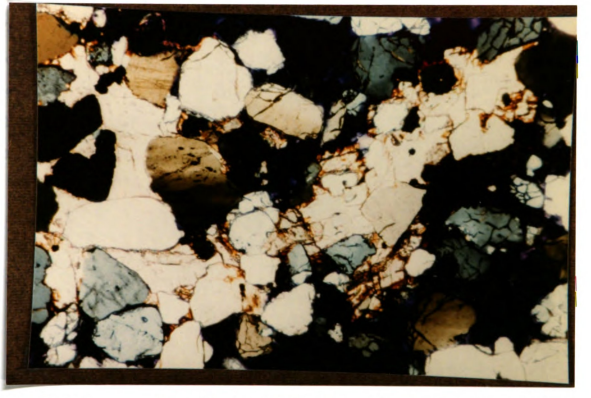

Figure 13. (b) Photomicrograph of subsurface "pre-weathering" carbonates displaying both poikilitic carbonate and rhombs. U.S.G.S. sample S13-51. Crossed-polars; field of view is 2.9 mm across. (Photo courtesy of U.S. Geological Survey, Lansing, Michigan).

Quartz

Subsurface quartz grains may be found rounded, as well as euhedral. Several photomicrographs show vermicular kaolinite, illite, and chlorite "growing out of quartz grains" (Westjohn, written communication) (Figure 15). Outcrop samples may be found containing vermicular molds, sometimes goethite filled. This observation suggests that quartz either contained chlorite in the source region, or diagenetically altered to chlorite, which in turn is being weathered to goethite, or being completely dissolved (Figure 15b).

K-Feldspar

Feldspars in the subsurface are characterized by being altered by carbonate. Microcline may be found very altered (often with etch pits), sometimes to vermicular clays. In general, feldspar is very similar between outcrop and subsurface (appears stable), which is reflected in the point count data (Tables 2 & 3) (Figure 7). This stability is very intriguing in that muscovite shows evidence of dissolution and alteration (Figure 8), yet has a dissolution rate constant in the laboratory nearly one order of magnitude lower than that for K-feldspar (Busenberg & Clemency, 1976; Lin & Clemency, 1981).

Clay Minerals

Clays frequently occur as pore fillings of kaolinite and illite in the subsurface, exactly like that found in outcrop, except dissolution of the clay is apparent in outcrop (Figure 10). Absent in outcrop is abundant illite cement with a

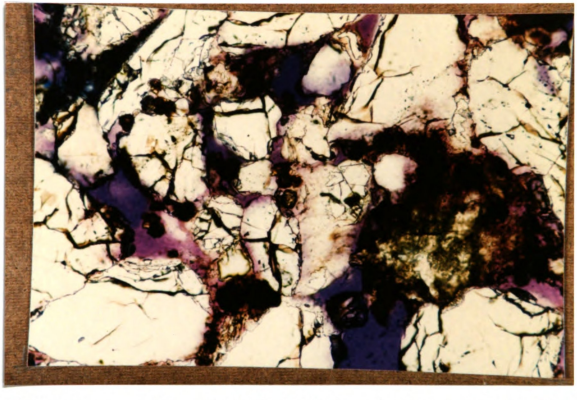

Figure 14. (a) Photomicrograph showing iron-bearing carbonates altering to iron oxy-hydroxides in the subsurface. U.S.G.S. sample S3-41. Plane-polarized light; field of view is 1.00 mm across. (Photo courtesy of U.S. Geological Survey, Lansing, Michigan).

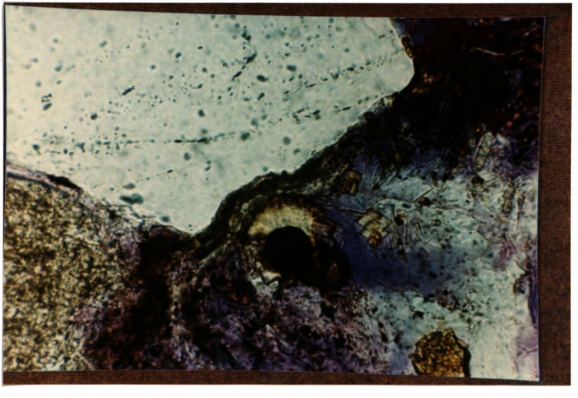

Figure 14. (b) Photomicrograph showing iron-bearing carbonates altering to iron oxy-hydroxides in the subsurface. U.S.G.S. sample B2-76. Crossed-polars; field of view is 0.5 mm across. (Photo courtesy of U.S. Geological Survey, Lansing, Michigan).

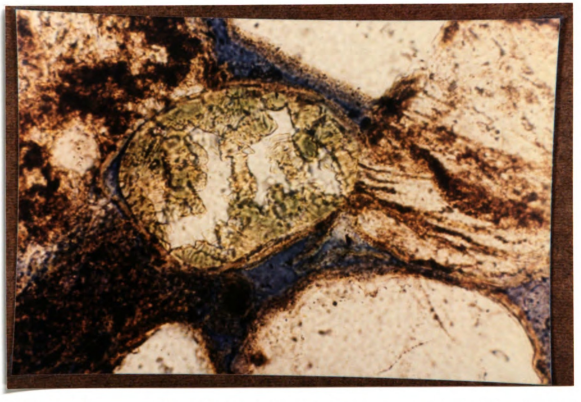

Figure 15. (a) Photomicrograph of a subsurface quartz grain altering to chlorite. U.S.G.S. sample J14-199. Plane-polarized light; field of view is 0.50 mm across. (Photo courtesy of U.S. Geological Survey, Lansing, Michigan).

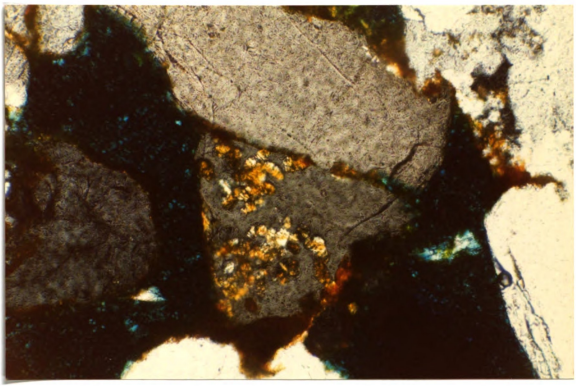

Figure 15. (b) Photomicrograph of the Eaton sandstone showing result of weathering the quartz-hosted chlorite in (a). Sample JP-95-13. Crossed-polars; field of view is 0.6 mm across.

fibrous habit growing perpendicular to grain surfaces. Kaolinite may be found inside pores, completely surrounded by carbonate. This kaolinite manifests itself in outcrop as vermicular books "floating" in the pores spaces.

Pyrite

Authigenic pyrite may be framboidal or occur as individual crystals in the subsurface. As stated earlier, only three euhedral grains were observed in the outcrop, compared to 2.7% of the total rock in the subsurface (Westjohn, written communication). It is likely that the pyrite is also a contributor of iron for goethite formation. In addition, pyrite oxidation is likely responsible, at least in part, for producing the acidic conditions which are dissolving the carbonate. This idea will be investigated further in the mass balance section of this thesis. The reader is referred to page 12 for a discussion of pyrite weathering.

Ferruginous Oxy-Hydroxides

Subsurface thin sections generally contain relatively little iron oxy-hydroxides. However, one thin section observation records heavy iron oxide in pores, some nearly spherulites, and related to carbonate cement (Westjohn, written communication) (Figure 14). Hematite is observed in the subsurface, but is scarce, and is not unequivocally identified. Otherwise, all subsurface ferruginous oxy-hydroxides are associated with carbonate dissolution.

CHAPTER 3: CLAY MINERALOGY

METHODS

Five samples were chosen for XRD identification of clays and oxy-hydroxides. Two of these were taken from the freshest outcrop (JP-95-21 and JP-95-17), and the remaining three were sampled from each of the other outcrop locations.

Four oriented mounts of each sample were prepared, one saturated with potassium, one saturated with magnesium, one saturated with magnesium and glycolated at room temperature, and one with only the naturally-occurring exchange ions. After the initial XRD analyses, the potassium-saturated samples were heated to 575° C, and rescanned. Scans were made on a Rigaku "Geigerflex" x-ray diffractometer system from 2° to 35° 2θ, at 35 kV, 25 mA, with a scan rate of 1° 2θ/minute, and divergence, receiving, and scatter slits were 1/6°, 0.3 mm, and 2°, respectively, using Ni-filtered CuKα radiation. Complete clay-mineral preparation techniques may be found in Appendix D.

RESULTS

The results of the XRD analyses of the samples are summarized in Table 5, and selected diffractograms are located in Appendix A. No attempt has been made to quantify the clay phases, but the diffractograms may suggest the relative abundance or degree of crystallinity; that is, the sharper and taller the peak, the more abundant and/or the better crystallized the clay.

The freshest samples (JP-95-21 and JP-95-17) show the presence of vermiculite, illite, kaolinite, and goethite. No chlorite or carbonate was found in any sample as reported by Martin (1982). Since no vermiculite has been identified in the subsurface (Table 1; Westjohn, written communication; Table 6), it may be concluded that it is a weathering product. Furthermore, since vermiculite is absent from the more intensely weathered samples, increased weathering appears to be removing this phase. The vermiculite parent is believed to be muscovite, as stated previously.

Sample JP-95-10 is the most intensely weathered sample, and petrographically contains the most abundant limonite. Not surprisingly, the XRD analyses for this sample exhibits the tallest and sharpest goethite peak of all the samples analyzed, and the kaolinite and illite peaks are not nearly as intense as the other samples (Appendix A). It may be concluded that weathering results in the removal and/or decreases the crystallinity of kaolinite and illite, and

increases the abundance and/or degree of crystallinity of goethite.

Table 5. Summary of XRD data from the outcrop Pennsylvanian Eaton sandstone.

Sample	Mineralogy
JP-95-2	Kaolinite, illite, goethite, vermiculite
JP-95-10	Kaolinite, illite, goethite
JP-95-13	Kaolinite, illite, goethite
JP-95-17	Kaolinite, illite, goethite, vermiculite
JP-95-21	Kaolinite, illite, goethite, vermiculite

Table 6. Summary of U.S.G.S. subsurface Pennsylvanian sandstone XRD data. (From Westjohn, written communication).

Sample	Mineralogy
72	Kaolinite >>> illite
80	Kaolinite >> illite, trace chlorite
85	Kaolinite >> illite, trace chlorite
93	Kaolinite >> illite, trace chlorite
106	Kaolinite >>> illite
110	Kaolinite >>> illite, trace chlorite
121	Kaolinite >>> illite, hint chlorite
125	Kaolinite >>> illite, hint chlorite
127	Kaolinite > illite, trace chlorite
133	Kaolinite >> illite, trace chlorite
134	Kaolinite >>> illite, hint chlorite
PSS-1	Kaolinite >> illite, hint chlorite
PSS-3	Kaolinite >> illite, trace chlorite
PSS-2	Illite > kaolinite, minor chlorite
JS-1	Kaolinite > illite, minor chlorite
JS-4	Kaolinite = illite, minor chlorite
JS-5	Kaolinite = illite, minor chlorite
JS-6	Illite = kaolinite, minor chlorite
JS-8	Kaolinite > illite, minor chlorite
JS-9	Kaolinite > illite, minor chlorite
JS-10	Kaolinite > illite, minor chlorite
JS-11	Kaolinite > illite, minor chlorite
JS-13	Kaolinite > illite, minor chlorite
JS-14-1	Kaolinite > illite, trace chlorite
USGS 110	Kaolinite, minor illite, trace chlorite
USGS 106	Kaolinite, minor illite, trace chlorite
USGS 52	Kaolinite, trace illite

CHAPTER 4: MASS BALANCE MODELING

METHOD OF CALCULATION

The mass balance calculations performed in this study follows the method described by Merino (1975a, 1975b), and utilized by Land & Milliken (1981). It requires that molar volumes ($\bar{v}$) of all mineral phases used in the balance be known. The units of molar volume are cm^3/mol, the inverse of which (mol/cm^3) is desired in order to generate the number of moles released per given volume of rock (in this investigation the reference volume of rock for mass balance calculations will be cubic meters). The inverse molar volume, therefore, may be calculated using the following expression:

$$1/\bar{v} = G * (1/mw) * 10^6 \ cm^3/m^3$$

where $1/\bar{v}$ = the inverse molecular volume in mol/m^3,

G = the specific gravity of the mineral in g/cm^3 (all specific gravity values are taken from Klein & Hurlbut, 1985),

mw = the molecular weight of the mineral in g/mol.

The inverse molecular volumes used in the calculations of this communication may be found in Table 7.

The volume of a given mineral lost or gained during

weathering was determined by point counting, with the subsurface thin sections representing the pre-weathering mineral abundances. Approximately 80 Upper Pennsylvanian subsurface thin sections were examined in order to select those which texturally and compositionally match the outcrop. Only 12 of these thin sections were qualitatively and quantitatively similar enough to the outcrop to justify their use as pre-weathering representatives of the outcrop. The outcrop and subsurface sandstone detrital abundances are plotted in Figure 3. It should be noted that the subsurface samples are more lithic rich, departing from the quartz arenite classification and into the sublitharenite classification. The lithic fragments in the subsurface thin sections are typically schistose fragments; small polycrystalline and monocrystalline quartz grains bound by platy muscovite. In outcrop, these lithic fragments are manifested as clustered silt size quartz grains, separated by dissolution voids where muscovite once was, but has since been weathered away. It is possible that the outcrop rocks are simply a different lithofacies than the selected subsurface rocks (the most lithic rich subsurface rocks are from the "B" suite of Westjohn (written communication), while the remainder are from their "S" suite). However, the persistence of clustered silt size quartz grains observed in the subaerial samples suggests that the outcrop rocks may have been more lithic-rich prior to weathering. With the quartz and feldspar modal ranges being extremely similar between outcrop and

subsurface samples (Tables 2 & 3), the possibility that differences in primary depositional facies are responsible for the compositional variation observed in Figure 3 is very small, although not negligible. The author point-counted both the subsurface and the outcrop, the data and statistics of which may be found in Tables 2 & 3. At least 300 points were counted for each slide, with the final totals almost always equalling 400 points or more. The net loss or gain of each mineral may be found in Table 7.

The only mineral that was not actually point counted by the author is pyrite. All of the 12 subsurface thin sections are within 135 feet of the Earth's surface and are beginning to alter. All of the slides exhibit high porosity and some carbonate dissolution. Since pyrite is one of the most highly soluble minerals it has already been removed. However, Westjohn (written communication) reports a thin section containing 2.7% pyrite and 6% porosity. If it is assumed that the sandstone was completely occluded with cement prior to uplift, then the 6% porosity combined with the ease with which pyrite weathers suggests that even 2.7% is a minimum value. Furthermore, it is likely that pyrite weathering is responsible for producing the acid which, at least in part, is dissolving the carbonate. Therefore, the absence of pyrite in the 12 subsurface thin sections used in this study does not imply that no pyrite was precipitated, but, rather, that pyrite dissolution has already occurred.

With the molar volumes of each mineral calculated and the

percent change (created or destroyed) determined from point count data, the number of moles of a given mineral formed or removed from a cubic meter of rock may be determined. Before doing the elemental mass balance, however, accurate mineral compositions must be known, and balanced chemical reactions must be identified.

MINERAL COMPOSITIONS

Table 7 lists the mineral compositions used in the material balance calculations, and the sources of the formulas. Formulas are either idealized textbook formulas or actual formulas determined by quantitative energy dispersive spectroscopy (Westjohn, written communication).

Pyrite

Elemental stoichiometries of Fe^{2+} and S^{-} were determined by EDS to be FeS_2, the idealized textbook formula.

Carbonates

Westjohn (written communication) performed extensive analyses of the carbonate phases. Quantitative EDS data was conducted on carbonate patches, nearly all rendering very good major element oxide totals close 100%. Those analyses which did not sum to within ±1.5% of 100% were not used in this study.

The four carbonates found to be present in significant quantities are calcite (typically poikilotopic), ankerite, siderite, and dolomite. The exact modal distribution of each

has not been determined. However, when performing mass balance calculations the modal percent of each carbonate is needed. Based on the report by Westjohn (written communication), as well as petrographic observations made by the author, a geologically reasonable carbonate distribution may be established. Admittedly, this distribution makes a number of inferences, but nonetheless, the distribution is geologically reasonable, and is constrained by all available information. The constraints are summarized in Table 4. The information in Table 4 implies the following relationship between carbonates:

Ankerite > Siderite > Calcite > Dolomite

The siderite composition is actually an average since the siderite concretions are reported to be zoned from a Mg-poor core to a Mg-rich edge. The average is between the core and the edge ($Fe_{0.95}Ca_{0.02}Mn_{0.03}CO_3$ and $Fe_{0.80}Ca_{0.03}Mg_{0.14}Mn_{0.03}CO_3$, respectively). The total carbonate percentage is the subsurface modal carbonate + modal porosity, which assumes that all porosity in the subsurface samples resulted from the removal of carbonate cement (Table 3).

Kaolinite

The reported oxide abundances for kaolinite have extremely poor totals. The error is likely attributed to the inherent difficulty associated with analyzing any mineral composed of clay-size crystals, combined with the fact that EDS cannot determine the structural water content of hydrous

minerals. Since there is essentially no compositional variation in kaolinite, using an idealized formula is justified.

Goethite, Muscovite, and Quartz

No data is available on the true compositions of any of these phases. However, none of these minerals exhibits large stoichiometric variability in nature, and, therefore, traditional chemical formulas will be used for the material balance calculations.

Table 7. Mineral data for phases used in the mass balance model.

Phase	$1/\bar{v}$ (mole/m^3)	Chemical formula	Net loss or gain (%): Joint block interior	Joint face
Pyrite	$4.17*10^4$	$FeS_2^{\tau,\Phi}$	-2.7	-2.7
Calcite	$2.70*10^4$	$Ca_{0.97}Fe_{0.03}CO_3^{\Phi}$	-4.4	-4.4
Ankerite	$1.42*10^4$	$Ca_{1.1}Mg_{0.44}Fe_{0.46}(CO_3)_2^{\Phi}$	-7.3	-7.3
Siderite	$3.50*10^4$	$Fe_{0.87}Ca_{0.03}Mg_{0.07}Mn_{0.03}CO_3^{\Phi}$	-6.1	-6.1
Dolomite	$1.53*10^4$	$Ca_{0.98}Mg_{0.96}Fe_{0.06}(CO_3)_2^{\Phi}$	-3.3	-3.3
Goethite	$4.92*10^4$	α-$FeO(OH)^{\tau}$	+6.4	+19.7
Muscovite	$7.08*10^{3\text{☼}}$	$KAl_2(AlSi_3O_{10})(OH)_2^{\tau}$	-0.3	-0.3
Kaolinite	$1.01*10^4$	$Al_2Si_2O_5(OH)_4^{\tau}$	-0.5	-0.5
Quartz	$4.41*10^4$	SiO_2^{τ}	-1.8	-1.8

☼ The specific value of muscovite varies over a small range. In this case the geometric mean was used for the inverse molecular volume calculation.
τ Standard formula from Klein & Hurlbut, 1985.
Φ Microprobe data from Westjohn, written communication.

BALANCED CHEMICAL REACTIONS

As stated previously, balanced chemical reactions are needed to perform mass balance modeling. All of the chemical reactions used in this study are listed in Table 8.

Table 8. Chemical reactions used for mass balance modeling.

Reaction Title	Balanced reaction
Pyrite dis.	$FeS_2 + 3.5\ O_2 + H_2O \leftrightarrow Fe^{2+} + 2\ H^+ + 2\ SO_4^{2-}$
Calcite dis.	$H^+ + 0.88\ Ca_{0.97}Fe_{0.03}CO_3 \leftrightarrow 0.86\ Ca^{2+} + 0.03\ Fe^{2+} + 0.12\ H_2CO_3 + 0.76\ HCO_3^-$
Ankerite dis.	$H^+ + 0.44\ Ca_{1.1}Mg_{0.44}Fe_{0.46}(CO_3)_2 \leftrightarrow 0.49\ Ca^{2+} + 0.20\ Fe^{2+} + 0.19\ Mg^{2+} + 0.12\ H_2CO_3 + 0.764\ HCO_3^-$
Siderite dis.	$H^+ + 0.88\ Fe_{0.87}Ca_{0.03}Mg_{0.07}Mn_{0.03}CO_3 \leftrightarrow 0.77\ Fe^{2+} + 0.03\ Ca^{2+} + 0.06\ Mg^{2+} + 0.03\ Mn^{2+} + 0.12\ H_2CO_3 + 0.76\ HCO_3^-$
Dolomite dis.	$H^+ + 0.44\ Ca_{0.98}Mg_{0.96}Fe_{0.06}(CO_3)_2 \leftrightarrow 0.43\ Ca^{2+} + 0.03\ Fe^{2+} + 0.42\ Mg^{2+} + 0.12\ H_2CO_3 + 0.76\ HCO_3^-$
Goethite precip.	$Fe^{2+} + 0.25\ O_2 + 1.5\ H_2O \leftrightarrow \alpha FeO(OH) + 2\ H^+$
Muscovite dis.	$KAl_2(AlSi_3O_{10})(OH)_2 + 12\ H_2O \leftrightarrow K^+ + 3\ Al(OH)_4^- + 3\ H_4SiO_4 + 2\ H^+$
Kaolinite dis.	$Al_2Si_2O_5(OH)_4 + 7\ H_2O \leftrightarrow 2\ Al(OH)_4^- + 2\ H_4SiO_4 + 2\ H^+$
Quartz dis.	$SiO_2 + 2\ H_2O \leftrightarrow H_4SiO_4$

Carbonate Equilibria

Since carbonate dissolution is both temperature and pH dependent, it deserves special attention (Drever, 1988). In finding the appropriate pH for carbonate dissolution due to pyrite weathering, subsurface water chemistry was found which had high dissolved Fe^{2+}, high dissolved sulfate, and high alkalinity (Dannemiller & Baltusis, 1990). In doing so, the

idea is to find those wells where pyrite oxidation appears to be occurring, and average those pH and temperature values in order to determine the CO_3 and bicarbonate (HCO_3^-) concentration in the weathering waters. The average values finally used were based on 12 wells, which average a pH of 7.25, and a temperature of 12.42° C. Using the following general reaction:

$$2\ H_2CO_3 \overset{K_1}{\leftrightarrow} 2\ H^+ + 2\ HCO_3^-$$

which may be written as follows:

$$4\ H^+ + 2\ CaCO_3 \leftrightarrow 2\ H^+ + 2\ HCO_3^- + 2\ Ca^{2+}.$$

The dissociation reaction of bicarbonate is not important here since the pH is 7.25. Since, the equilibrium constant K_1 varies linearly with temperature at temperatures below approximately 25° C, then K_1 may be extrapolated from Drever's (1988) data. At 12.42° C, the equilibrium constant K_1 equals $3.63*10^{-7}$.

If $K_1 = [H^+][HCO_3^-]/[H_2CO_3]$, then $K_1/[H^+] = [HCO_3^-]/[H_2CO_3]$

$= 3.63*10^{-7}/5.62*10^{-8}$

$= 6.46/1$

Therefore, at pH = 7.25 and T = 12.42° C, inorganic carbon is

distributed between the following species:

$$0.87\ HCO_3^-$$

$$0.13\ H_2CO_3$$

which provides:

$$2\ H_2CO_3 \leftrightarrow 0.27\ H_2CO_3 + 1.73\ H^+ + 1.73\ HCO_3^-$$

Calcite dissolution involves a net 2.27 H^+, and the overall reaction becomes:

$$H^+ + 0.88\ CaCO_3 \leftrightarrow 0.12\ H_2CO_3 + 0.88\ Ca^{2+} + 0.76\ HCO_3^-.$$

It must be kept in mind that the above solution is the general case for the dissolution of any carbonate.

Silica Equilibria

Silica solubility, too, involves the production of the weak monosilicic acid (H_4SiO_4). However, in this case, H_4SiO_4 is not particularly problematic because measured pH values of spring water draining the Eaton sandstone show a pH of 8.8, and at pH below about 9 only H_4SiO_4 contributes significantly to the ΣSi (Richardson & McSween, 1989). Therefore, the simple congruent reaction of silica and water in Table 8 is sufficient here.

Aluminosilicate Solubility

The aluminosilicate minerals involved in the mass balance calculations are muscovite and kaolinite. What is important about these two phases is that the aqueous aluminum species resulting from their dissolution is pH dependent (Drever,

1988). At an outcrop pH of 8.8, $Al(OH)_4^-$ will be the dominant aqueous aluminum species (Drever, 1988), which is reflected in the chemical reactions in Table 8.

ION MASS BALANCE

With balanced precipitation and dissolution reactions identified from thin sections (Table 8), and modes of new and destroyed minerals determined (Table 7), quantities of each element imported and exported for a given volume of rock may be established (Table 9).

Table 9. Mass balance calculations for joint face and joint block interior. (All abundances in moles/m^3 of sandstone.)

A. JOINT FACE

	% of	Moles needed		Moles released								
Phase	rock	H^+	Fe^{2+}	H^+	Fe^{2+}	Si^{4+}	Ca^{2+}	Mg^{2+}	Mn^{2+}	Al^{3+}	K^+	SO_4^{2-}
Pyrite	-2.7			2300	1100							2300
Calcite	-4.4	1300			35		1200					
Ankerite	-7.3	2300			470		1100	450				
Siderite	-6.1	2400			1900		63	150	63			
Dolomite	-3.3	1100			29		490	480				
Goethite	+19.7		10300	20700								
Muscovite	-0.3			42		64				64	21	
Kaolinite	-0.5			100		100				100		
Quartz	-1.8					790						
Totals		7100	10300	23142	3534	954	2853	1080	63	164	21	2300

B. JOINT BLOCK INTERIOR

	% of	Moles needed		Moles released								
Phase	rock	H^+	Fe^{2+}	H^+	Fe^{2+}	Si^{4+}	Ca^{2+}	Mg^{2+}	Mn^{2+}	Al^{3+}	K^+	SO_4^{2-}
Pyrite	-2.7			2300	1100							2300
Calcite	-4.4	1300			35		1200					
Ankerite	-7.3	2300			470		1100	450				
Siderite	-6.1	2400			1900		63	150	63			
Dolomite	-3.3	1100			29		490	480				
Goethite	+6.4		3100	6300								
Muscovite	-0.3			42		64				64	21	
Kaolinite	-0.5			100		100				100		
Quartz	-1.8					790						
Totals		7100	3100	8742	3534	954	2853	1080	63	164	21	2300

Modal Mineral Changes

The point count data in Tables 2 & 3 includes maximum, minimum, and average values. In performing material balance only two numbers for a given mineral are needed; a pre-weathering percentage and a present day percentage. In this study, the author has elected to use average values from the point count data for several reasons. First, choosing the minimum values often provides 0% of a phase which is known to be present. For example, the minimum goethite value is zero, which is certainly not geologically reasonable for the Eaton sandstone. If one chooses the maximum values, then suddenly almost 2/3 of the original pore space is now occluded by goethite, which, again, is neither consistent with petrographic observations, nor is geologically reasonable. Therefore, this study utilizes mean modal mineralogies for the material balance calculations, which are the most reasonable based on petrographic and field observations. The "Net Loss or Gain" column in Table 5 is based on the mean values from Tables 2 & 3.

Precipitation Inputs

When performing any mass balance calculation both inputs and outputs must be identified. Since precipitation provides an input into this system of study, its chemistry becomes very important. Bulk precipitation chemical analyses were performed in Lansing, Michigan (11 miles east of Grand Ledge) (Peters & Bonelli, 1982), and East Lansing (Wood, 1969) (Table 10). Compared to the contributions of ions by the minerals,

the precipitation inputs are negligible. Admittedly hydrogen ion is present in the precipitation in significant quantities, but this study does not attempt to mass balance protons.

Sulfate is significantly concentrated in the precipitation of south central Michigan. In fact, the groundwater chemistry for one of the wells near Grand Ledge (Table 13) has a sulfate concentration exactly the same as the Lansing precipitation measurement (2.3 mg/l). At least for that particular well, precipitation is the only source of sulfate at the present time.

Table 10. Precipitation data from Lansing and East Lansing, Michigan. (All concentrations in mg/l.)

Specific Conductance (µs/cm)	pH	Ca^{2+}	Mg^{2+}	Na^{+}	K^{+}	SO_4^{2-}	Cl^{-}	Si^{4+}	Fe^{2+}	Mn^{2+}
☼ 13.0	5.34	0.39	<0.1	<0.2	<0.1	2.3	0.61	<0.01	0.02	0.004
▲ <50	5.8	10	0	--	--	3.5	0.8	--	--	--
▲ <50	5.3	10	0	--	--	2.0	0.9	--	--	--

☼ Peters & Bonelli, 1982
▲ Wood, 1969

An attempt was made to quantify the ionic inputs from precipitation through time into the Eaton sandstone, but such calculations are very complicated and elusive. In order to perform such calculations one needs to know the time of exposure of the outcrop, the change in porosity as a function of time, the changes in precipitation volume and chemistry as a function of time, the actual volume of precipitation to enter the rock, and whether evapotranspiration effects are causing increase in elemental concentrations. Obtaining

accurate numbers on the above is extremely difficult, and is beyond the scope of this thesis. However, it does suffice to conclude that the contributions of elements from precipitation is extremely small compared to the contributions from the weathering minerals. Wood (1969) came to the same conclusion for the Grand Ledge area. Furthermore, Wood (1969) states that chloride is the only major ion for which precipitation may be a significant source. Since chloride is not one of the elements involved in the material balance calculation, quantifying precipitation inputs is not necessary.

Joint Face vs. Joint Block Interior

The mass balance calculations were performed for both the joint face (1 cm thick), and the joint block interior (Table 9). It is apparent in the field that the 1 cm joint faces are much better indurated than the much more friable joint block interiors. Figure 16 shows a plot of modal percent goethite vs. distance from joint face, and what is readily apparent is the abundances of goethite in the 1 cm thick joint face. Furthermore, Table 9 shows that the joint faces behave as net importers of iron, while the joint block interior behaves as a net exporter.

For the diffusion of iron to occur to the joint face the sandstone must have been completely, or nearly completely saturated with water. This suggests that the formation of goethite occurred in the shallow subsurface, likely in the saturated zone. In addition, jointing must have occurred prior to pyrite oxidation and carbonate dissolution, since

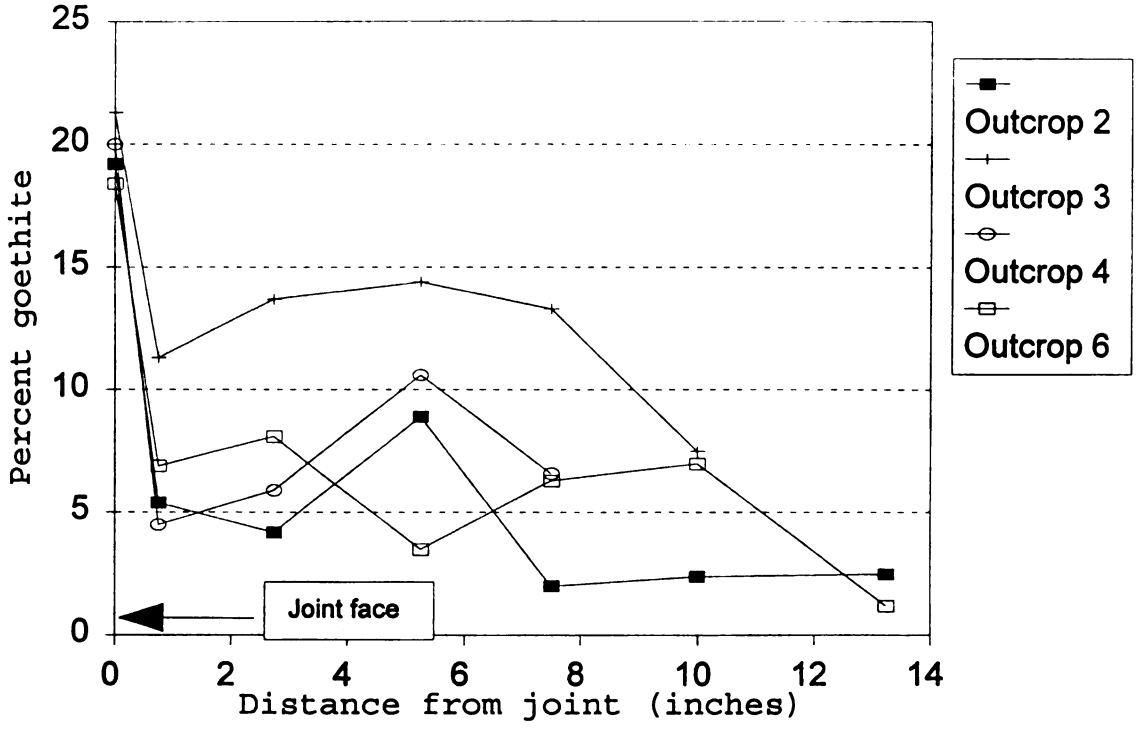

Figure 16. Percent goethite vs. distance from joint face.

these phases are the iron source. The idea that perhaps these outcrop sandstones may not have been buried sufficiently deep to achieve the subsurface diagenetic mineralogy should also be dismissed since significant burial, and resulting pressure, must have occurred to permit fracturing during uplift. This uplift and epidiagenetic sequence is supported petrographically. Subsurface thin sections exhibit initial pyrite oxidation, followed by carbonate dissolution. Table 9, however, shows that insufficient H^+ is released by pyrite weathering to dissolve all of the carbonate. Carbonic acid resulting from CO_2 dissolution in rainwater is the likely other acid responsible for carbonate dissolution. It is reasonable to conclude that groundwater flow along subsurface joint planes provided the oxidant responsible for the goethite formation at the joint faces (groundwater ferricretes).

The iron mass balance suggests that the Eaton sandstone is behaving as a closed system with respect to iron. The joint faces require approximately 6766 moles of Fe^{+2} per m^3 of sandstone more than they themselves can supply, while the joint block interiors release approximately 434 moles of Fe^{+2} per m^3 of sandstone than their secondary minerals need. These numbers indicate that each unit volume of case-hardened joint face material requires the importation of Fe^{+2} equivalent to that derived from over 15.5 unit volumes of joint block interior material.

COMPARISON WITH SUBSURFACE WATER CHEMISTRY AND MINERALOGY

Mass balance tabulations represent net import and export of ions through time. Any water chemistry data collected at the present represents the concentration of elements in solution at an instant in time. Therefore, a comparison of water chemistry over time (the mass balance) and instantaneous water should provide insight into the epidiagenetic sequence.

Mineral Stability

Table 11 provides a comparison of mineral stability for outcrop, glacial till aquifers (Wahrer, 1993), and Pennsylvanian aquifers (Meissner, 1993) in the Michigan basin. The stability of several of these phases deserves special attention.

Quartz

Outcrop petrography reveals quartz grains which are embayed, and particularly angular when bounding pores (Figure 6). An analysis of spring water draining the outcrop reveals SiO_2 concentrations of 5.62 mg/l (Beals, personal communication). Such a concentration reflects quartz saturation, and is typical for Earth's surface conditions (Krauskopf, 1956; Siever, 1962). As discussed earlier, initial quartz dissolution occurred in response to goethite precipitation. Today, however, it is simply the rain water attempting to reach saturation with respect to quartz, and may or may not be a result of the percolating waters having a pH of 8.8.

Table 11. Mineral stability comparison for outcrop, glacial till, and Pennsylvanian aquifers.

Mineral	Outcrop	*Glacial Till Aquifer	**Pennsylvanian Aquifer
Calcite	Unstable	Stable	Stable
Dolomite	Unstable	Slightly Unstable	Slightly Unstable
Gypsum	Unstable	Unstable	Unstable
Anhydrite	Unstable	Unstable	?
Quartz	Unstable	Stable	Stable
Illite	Unstable	Stable	Unstable
Kaolinite	Unstable	Stable	Stable
Muscovite	Unstable	Unstable	Stable
K-Feldspar	Stable (?)	Unstable	Unstable

* Wahrer, 1993
** Meisner, 1993

K-Feldspar

K-feldspar petrographically appears stable. Qualitatively the subsurface feldspar is as altered as that of the outcrop. Point count data reveals no loss of feldspar due to weathering (Tables 2 & 3). However, glacial till aquifer waters (Wahrer, 1993), and Pennsylvanian aquifer waters (Meissner, 1993) are undersaturated with respect to K-feldspar. Numerous physical and chemical conditions may explain the outcrop stability (e.g. water contact times, high pH, volume of water contacting the sandstone, etc.), but regardless of these conditions both kaolinite and muscovite show evidence of leaching.

Sulfate

Both Meissner (1993) and Wahrer (1993) believe that the sulfate in Pennsylvanian and glacial till aquifers, respectively, is from gypsum ($CaSO_4 \cdot 2H_2O$) and anhydrite ($CaSO_4$) weathering in overlying Jurassic red beds (Cohee, 1965). Any sulfate found in the water of the Upper Pennsylvanian aquifers of south central Michigan is not believed to be from red beds, but rather from pyrite oxidation. The maximum value of sulfate found in the waters of either the Saginaw or Grand River formations near Grand Ledge is 160.00 mg/l (Table 13), which may be entirely accounted for by oxidizing 2.7% pyrite. Therefore, when comparing outcrop mass balance calculations to shallow water chemistry, it may be assumed that the only elemental inputs into the aquifer are from precipitation and mineral-water interactions occurring within the Pennsylvanian recharge beds.

Long Term vs. Instantaneous Water Chemistry

Method

The mass balance calculations for the outcrop sandstone represent elemental imports and exports since the onset of weathering, and, therefore, may provide a way to estimate an average long term water chemistry. Since SiO_2 concentrations for a spring draining the outcrop are known, a normalization factor may be calculated and used to convert all of the other major ions into concentrations in mg/l. The method begins by taking the known, contemporary SiO_2 concentration of spring water and converting this concentration from mg/l to mol/l.

To do so, simply multiply the known SiO_2 concentration (5.62 mg/l; Beals, personal communication) by the molecular weight of quartz in milligrams (1 mol/60080 mg):

$$5.62 \text{ mg/l} * 1 \text{ mol}/60080 = 9.35*10^{-5} \text{ mol/l}.$$

Now that the concentration of SiO_2 is in mol/l, it may be divided by the number of moles of SiO_2 per m^3 of sandstone from the mass balance (Table 9) in order to clear the moles and leave units of m^3 of sandstone per liter (m^3 ss/l):

$$9.35*10^{-5} \text{ mol/l} \div 954 \text{ mol}/m^3 \text{ ss} = 9.81*10^{-8} \ m^3 \text{ ss/l}.$$

$9.81*10^{-8}$ m^3 ss/l is the conversion factor used to convert the mass balance values in moles per m^3 of sandstone (Table 9) into concentrations in mg/l. The conversion factor is the inverse of the volume of water (with the measured dissolved SiO_2 concentration) required to flush a cubic meter of sandstone to remove the amount of silica calculated by the mass balance (Table 9). If it is assumed that all solid phases in the sandstone have interacted with this same volume of water, then by multiplying the quantity of each element/specie in Table 9 (in mol/m^3 ss) by the conversion factor (in m^3 ss/l) a value in mol/l may be obtained. A concentration in mol/l is easily converted into mg/l by using the molecular weight of the particular element/specie and converting from grams to milligrams. For example, Ca^{2+} is as

follows:

$2853\ mol/m^3\ ss * 9.81*10^{-8}\ m^3\ ss/l = 2.8*10^{-4}\ mol/l$
(From Table 9) (conversion factor)

$2.8*10^{-4}\ mol/l * 40.08\ g/mol * 1000\ mg/g = 11.2\ mg/l$
(molecular weight)

The last value (11.2 mg/l) is placed in the "Outcrop (average over time)" column of Table 14. Iron is neglected from these calculations because of the difficulty involved in calculating the volume of the joint face, the volume of the joint block interior, the volume of the weathered skin, and the amount leached away, all of which are needed in order to sum the total number of moles of iron.

The "Subsurface (Present)" column of Table 14 is the major element water chemistry data from Upper Pennsylvanian aquifers near Grand Ledge, Michigan. Ratios are used for comparisons since the groundwater has undergone a longer flow path and has accumulated more solutes. When possible, data from the Grand River formation is used, however, data does not exist for all elements, in which case, Saginaw aquifer data is used. When comparing the Grand River data and Saginaw data (Tables 12 & 13), significant differences exist. For example, Grand River aquifer wells are shallower and more dilute. However, concentrations do not vary by orders of magnitude and, as will soon be seen, return very useful results.

Table 12. Water chemistry data from the Grand River aquifer near Grand Ledge, Michigan. (All concentrations in mg/l.)

Reference Identifier	Well Depth (feet)	Specific Conductance (µs/cm)	pH	Ca^{2+}	Mg^{2+}	Na^{+}	K^{+}	Alkalin. ($CaCO_3$)	SO_4^{2-}	Cl^{-}	TDS	Fe^{2+}	HCO_3
°CLIN55	137	--	--	--	--	--	--	102	12.0	3.0	--	0.36	230
°CLIN56	120	--	--	--	--	--	--	342	13.0	1.0	--	2.40	410
°KENT20	107	--	--	--	--	--	--	276	40.4	3.0	--	1.15	312
*CLINGR1	180	--	7.5	60	26.0	14.0	1.9	330	11.0	1.2	288	0.73	351
*CLINGR2	120	625	7.6	--	--	--	--	--	13.0	1.0	--	2.40	410
*CLINGR3	200	--	7.3	70	32.0	13.0	2.4	306	11.0	1.2	325	0.25	397
*CLINGR4	200	--	7.5	77	36.0	13.0	2.2	340	9.0	1.0	377	1.40	480
*CLINGR5	255	--	7.3	56	26.0	16.0	2.0	288	7.0	1.0	288	2.40	361
*CLINGR6	180	--	7.4	82	34.0	16.0	1.8	345	19.0	2.1	363	3.50	471
*CLINGR7	230	--	7.6	62	18.0	30.0	2.6	238	9.0	1.5	280	0.20	316
*CLINGR8	250	--	7.6	79	24.0	6.5	1.8	296	7.0	1.0	313	1.80	390
*CLINGR9	135	--	7.8	84	31.0	13.0	3.4	337	36.0	3.5	374	1.20	407
*CLINGR10	230	--	7.5	82	29.0	15.0	1.4	324	23.0	6.3	358	2.80	402
*CLINGR11	137	381	7.9	--	--	--	--	102	12.0	3.0	--	3.60	230
*CLINGR12	200	653	7.3	79	32.0	14.0	1.4	329	24.0	10.0	359	1.00	398
*CLINGR13	71	487	7.3	67	22.0	8.6	1.1	258	11.0	0.0	285	0.38	325
*CLINGR14	209	344	7.7	35	8.8	28.0	3.1	124	5.2	0.0	208	0.34	220
*EATOGR1	111	--	7.8	75	30.0	8.0	2.8	325	24.0	4.4	323	2.40	354
Mean	171	498	7.5	70	27.0	15.0	2.2	274	15.9	2.5	319	1.57	359
Stand. Dev.	55	139	0.2	14	7.4	6.9	0.7	84	10.0	2.5	49	1.13	76
Minimum	71	344	7.3	35	8.8	6.5	1.1	102	5.2	0.0	208	0.20	220
Maximum	255	653	7.9	84	36.0	30.0	3.4	345	40.4	10.0	377	3.60	480

° State of Michigan, 1966
* Wood, 1969
CLIN = Clinton County
EATO = Eaton County
KENT = Kent County

SiO_2, Ca^{2+}, Mg^{2+}, SO_4^{2-}

One way to check the data is to calculate the ratio of the elemental concentrations against SiO_2 for both outcrop and subsurface. This is the column entitled "Species/SiO_2" in Table 14. Notice how SiO_2, Ca^{2+}, Mg^{2+}, and SO_4^{2-} all show very similar numbers for outcrop and subsurface (within the same order of magnitude). This similarity suggests that the minerals which contain those species (quartz, ankerite/siderite/dolomite, ankerite/siderite/dolomite/calcite, and pyrite, respectively) are weathering at present in the shallow Upper Pennsylvanian aquifers. Notice, too, for these same species the similarity between the ratio of the long term average to the present (Table 14, column 6), as well as them all having a negative

Table 13. Water chemistry data from the Saginaw aquifer near Grand Ledge, Michigan. (Data from Dannemiller & Baltusis, 1990; All concentrations in mg/l.)

Reference Identifier	Well Depth (Feet)	Specific Conduct. (µs/cm)	pH	Ca^{2+}	Mg^{2+}	Na^{+}	K^{+}	Alkalin. ($CaCO_3$)	SO_4^{2-}	Cl^{-}	Si^{4+}	TDS	Al^{3+}	Fe^{2+}	Mn^{2+}
CLIN1	200	660	7.1	85	33	6.8	1.8	520	2.3	1.1	13	360	<0.01	0.66	0.02
CLIN2	305	557	7.4	69	32	13.0	2.2	316	8.4	1.2	18	316	<0.01	0.53	0.01
CLIN3	155	505	7.5	62	24	20.0	1.6	283	4.8	1.3	17	281	<0.01	0.23	0.19
CLIN4	462	556	7.2	71	26	11.0	2.6	297	17.0	2.6	9	324	<0.01	0.43	0.02
CLIN6	355	642	7.6	78	32	12.0	1.8	362	10.0	1.5	15	344	<0.01	0.56	0.02
EATO14	360	634	7.3	78	27	20.0	2.3	320	32.0	9.6	13	372	<0.01	0.44	0.01
EATO16	440	821	7.1	110	35	17.0	1.2	352	63.0	33.0	17	511	<0.01	1.10	0.04
EATO17	441	870	7.1	110	38	16.0	1.3	398	80.0	29.0	18	500	<0.01	1.10	0.05
INGH20	160	589	7.5	77	26	3.7	1.6	312	5.9	1.7	13	306	<0.01	0.71	0.02
INGH26	490	652	7.3	86	26	13.0	2.2	300	26.0	20.0	12	356	<0.01	0.51	0.02
IONI4	245	601	7.5	73	29	9.4	1.0	314	11.0	1.1	18	320	<0.01	0.90	0.03
IONI8	485	551	7.4	76	29	16.0	1.9	333	5.9	9.3	17	338	0.01	0.78	0.03
IONI9	450	774	7.5	120	37	40.0	3.4	367	160.0	21.0	12	590	<0.01	3.20	0.07
Mean	350	647	7.3	84	30	15.2	1.9	344	32.8	10.2	15	378	<0.01	0.86	0.04
Std. Dev.	125	111	0.2	18	5	8.9	0.6	62	45.1	11.6	3	94	0.00	0.75	0.05
Minimum	155	505	7.1	62	24	3.7	1.0	283	2.3	1.1	9	281	<0.01	0.23	0.01
Maximum	490	870	7.6	120	38	40.0	3.4	520	160.0	33.0	18	590	0.01	3.20	0.19

CLIN = Clinton County
EATO = Eaton County
INGH = Ingham County
IONI = Ionia County
The number following the four letter county abbreviation refers to the well number in Dannemiller & Baltusis (1990).

Table 14. Long term vs. present day water chemistry in Pennsylvanian sandstones. (All concentrations in mg/l.)

Species	Outcrop (Long Term)	Subsurface (Present)	Species/SiO_2 Outcrop	Species/SiO_2 Subsurface	Long Term/Present	Long Term-Present
SiO_2	5.6	15*	1	1	0.38	-9.2
Ca^{2+}	11.2	70	2.0	4.7	0.16	-58.8
Mg^{2+}	2.58	27	0.46	1.8	0.10	-24.4
Mn^{2+}	0.34	0.04*	0.06	0.003	8.5	+0.3
Al^{3+}	0.43	<0.01*	0.08	0.01	<43	+0.42
K^{+}	0.08	2.2	0.01	0.15	0.04	-2.12
SO_4^{2-}	1.55	15.9	0.28	1.1	0.10	-14.35

*Data taken from the Saginaw aquifer (Table 13) rather than the Grand River aquifer.

difference when subtracting the present from the long term average (Table 14, column 7).

It may seem strange that quartz dissolution appears to be occurring in the Pennsylvanian aquifer when Meissner (1993) reported that quartz is stable in these aquifers. It must be remembered that the water chemistry data acquired for this comparison are from the shallowest, most dilute aquifers where weathering is likely occurring. Meissner's (1993) mineral stability data is for the entire Michigan basin which includes

a large number of relatively deep, solute-rich wells. In summary, the wells utilized in this study are sufficiently shallow to reside above the weathering front, permitting minerals like quartz and carbonate to experience weathering, while Meissner (1993) incorporates numerous, very deep, solute-rich wells into his study, which is a generalization of the entire Michigan basin.

K^+

Potassium, too, has a negative value in column 7 of Table 14, but columns 4 and 5 (ratio of chemical species to SiO_2) differ by 15 times. The fact that the $[K^+]/[SiO_2]$ ratio is smaller in outcrop than in the subsurface suggests that less dissolution of K^+-bearing minerals is occurring in outcrop. The possible K^+-bearing phases are K-feldspar and muscovite. According to Meissner (1993) muscovite is stable in the subsurface, while K-feldspar is unstable. Muscovite occurs in very small abundances in both outcrop and subsurface (mean of 0.1% and 0.4%, respectively) and is therefore, not a major contributor of potassium to either outcrop or aquifer. K-feldspar, in contrast, has a mean modal percent of 2% in the subsurface and outcrop (Tables 2 & 3). This relatively large K-feldspar abundance coupled with instability provides a substantial source for the potassium ion in the groundwater. Though in similar abundance in outcrop, the K-feldspar's apparent stability at the Earth's surface prevents significant K^+ from being leached from the weathering environment.

Mn^{2+} and Al^{3+}

Mn^{2+} and Al^{3+} also deserve explanation. For these two cations, column 7 in Table 14 is positive, indicating that they are being mobilized in outcrop more so than in the aquifers. It also implies that the phases in the subsurface which contain manganese and aluminum have either not commenced weathering (are stable), or have been completely removed by meteoric water.

The only source of Mn^{2+} is siderite. Westjohn (written communication) reports that for the most porous subsurface sandstones, the remnant carbonate is ankerite and/or calcite. The petrographic observations of this study confirm that statement. This implies that siderite is one of the earliest phases to dissolve. If so, then the very low subsurface Mn^{2+} concentrations likely reflect the complete absence of siderite in the present day, or, at least, a lack of Mn mobility. Since the water chemistry data used for this study is from shallow wells, the above discussion is altogether geologically reasonable.

Aluminum is particularly interesting. The primary sources of aluminum are muscovite and kaolinite. From Table 11 it is observed that both phases are stable in the subsurface, thus explaining the minimal Al^{3+} concentrations in the subsurface. In other words, subsurface Al^{3+}-bearing phases have not yet begun to weather. However, both muscovite and kaolinite are unstable in outcrop and are undergoing dissolution. What is of particular importance to note here is

that aluminum (and possibly manganese) is mobilizing in the outcrop sandstone.

CHAPTER 5: UNCONFORMITIES AND HYDROCARBON RESERVOIRS

The Eaton sandstone represents porosity enhancement as a result of acidic meteoric water leaching below a modern-day unconformity surface. Such porous weathered zones as this may provide potential hydrocarbon reservoirs if trapped beneath unconformities (Heald et al., 1979; Shanmugam, 1988, 1990; Shanmugam and Higgins, 1988). Furthermore, this study allows one to see first hand the secondary changes associated with weathering; such alterations are sometimes difficult to distinguish from deep diagenetic changes when studying subsurface unconformity surfaces (Heald et al., 1979).

This study found that other than the alteration of muscovite to vermiculite, the major chemical operator acting on the Eaton sandstone at the present time is dissolution. What is noteworthy, however, is that K-feldspar appears stable. Emery et al. (1990), for example, found that the abundance of potassium feldspar below an unconformity increased with depth, while the kaolinite abundance decreased with depth, suggesting potassium feldspar leaching by meteoric water resulted in concomitant kaolinite precipitation as a result of subaerial exposure. Chittleborough (1989), too, reports microcline altering to kaolinite in a soil developed on a feldspathic sandstone. Young (1986) had similar findings

for the Bungle Bungle Massif of Australia. An absence of kaolinite below the Cimmerian unconformity in the northern North Sea was explained by Bjorkum et al. (1990) to be the result of an erosion rate exceeding the propagation rate of the dissolution/weathering front. Such an explanation is inappropriate for explaining the absence of epidiagenetic kaolinite at Grand Ledge since the weathering zone is well preserved and erosion is at an absolute minimum. In addition, Arditto (1983) found kaolinite to be the major stable phase in the intake beds of the Great Australian basin, with K-feldspar and muscovite dissolution providing the ions for the kaolinite formation.

The reasons why K-feldspar may be stable, or metastable, in outcrop have already been discussed. Let it simply be stated here that the Eaton sandstone is a modern day exposure surface in which neither potassium feldspar is altering to kaolinite, nor is the erosion rate exceeding the propagation rate of the dissolution front. This study agrees with Bjorkum et al. (1990) who state that kaolinization may not be as important below unconformity surfaces as once was believed.

CHAPTER 6: HONEYCOMB WEATHERING

As mentioned earlier, honeycomb weathering is ubiquitous at Grand Ledge, and is apparently a function of the presence of salts on the outcrop surface, the aspect of the outcrop, and the massiveness of the sandstone (Wallis & Velbel, 1985). Mustoe (1982) attributed honeycomb weathering in coastal exposures of arkosic sandstones to the evaporation of salt water deposited by wave splash, an the resulting salt precipitation physically disaggregating the sand grains. This same researcher mentions that the cavity walls are not reinforced by the weathering skin (but rather green algae), which has been suggested by other researchers. Wave splash action has also been proposed for forming miniature pits in the quartz arenites of India (Ganesh & Sathyanarayan, 1991). Smith (1982) pays great tribute to Mustoe for taking such a scientific approach to honeycomb weathering, but, in as much as Smith approves of Mustoe's approach, he is quick to point out that honeycomb weathering occurs in other geographic regions besides the shoreline. In fact, Smith (1983) presents a NASA photograph of a Martian boulder on which resides honeycomb weathering!

The purpose of this section is not to provide an exhaustive review of the literature on honeycomb weathering,

but rather to make a comparison of the Grand Ledge honeycombing with other researchers work.

Robinson & Williams (1992) discuss the difficulty in finding an explanation for honeycombing. These researchers make the following observations about honeycomb weathering: concentrated along bedding planes, favored on massive joint blocks, and usually occur on the south and west sides of the joint blocks. These researchers propose that frost action, salt wedging, water seepage along bedding planes, and patchy protective crusts are all factors in the generation of honeycombs. These observation correspond with those made by Wallis & Velbel (1985).

Mustoe (1983) evaluated the honeycomb weathering at an inland locality, Capitol Reef Desert, Utah. He utilized chemical analyses, XRD data, and field observations to suggest that salt weathering is the most important cause of disintegration, possibly aided by calcite dissolution in the calcareous sandstones. Kelletat (1980) records the same observations for calcareous sandstones in western Scotland and southern Greece, for which honeycombs are full of sand and mixed with fine salt crystals. Such sandstones are, however, coastal, with saltwater spray reaching the honeycomb zone. In contrast, Gill et al. (1981) examined a honeycomb weathered greywacke with a scanning electron microscope (SEM), and found that salt was not associated with honeycombs, even though the honeycombs occurred in the supratidal zone where the rocks are frequently wet by sea spray.

Several researchers have suggested that mineral weathering is responsible for initiating honeycombing. Butler and Mount (1986) propose that the chemical dissolution of selected minerals (quartz, feldspar, and phyllosilicates), as well as salt-weathering and/or heat-moisture expansion processes resulting from splash-zone wetting and drying that produce the rock corrosion (honeycombing). Certainly quartz corrosion and phyllosilicate dissolution are occurring at Grand Ledge. Sancho and Benito (1990) suggest that for the Ebro basin of Spain, the initiation of honeycombing is related to the presence of easily weatherable minerals. It has also been reported that the shape of honeycombs depends on textural factors which control water circulation in the sandstone, which has a direct effect on feldspar hydrolysis, wetting-drying, and salt weathering (Sancho & Gutierrez, 1990). Young & Young (1992) also discuss the importance of sandstone permeability to honeycombing. They suggest that the reason honeycombs are ubiquitous in the Aztec sandstone and absent in the Navajo sandstone is because the Aztec sandstone contains significant porosity, while the Navajo sandstone contains large joints through which rainwater is funneled, preventing meteoric water from entering the interior of the joint blocks. Admittedly, the Eaton sandstone contains many joint surfaces. However, the large porosity and mineral dissolution associated with the Eaton sandstone suggests substantial infiltration of rainwater.

Finally, McGreevy (1985) reports the presence of gypsum

salts on the honeycombs of a Carboniferous sandstone in northern Ireland, as well as quartz etching, but is not sure if they influence honeycombing. He even states that the cause of honeycomb formation is not known.

This study has little to add to the already large body of observations made regarding honeycomb weathering. Grand Ledge honeycomb characteristics that have not been dismissed by other researchers are that they occur on massive very porous joint block interiors, and that quartz and phyllosilicate dissolution are occurring. The only study which did not find salts associated with honeycombing was Gill et al. (1981). Regardless, it is readily apparent that the cause of honeycomb weathering still eludes geomorphologists.

CHAPTER 7: SUMMARY AND CONCLUSIONS

SUMMARY

This study compares the weathering mineralogy of the subaerially exposed Pennsylvanian Eaton sandstone with the age-equivalent subsurface rocks found deeper in the Michigan basin. By comparing the effects of weathering with the pre-weathering mineralogy established from subsurface drill cuttings, this investigation has provided insight into the nature of porosity evolution below unconformities.

The hypothesis that the authigenic mineralogy of the Eaton sandstone may be explained in terms of an open chemical system is not entirely supported. It holds true to nearly all elements, except for iron, and possibly manganese. Admittedly, in the present day goethite dissolution is occurring. However, portions of the dissolved iron load are being reprecipitated as the weathering crust, as well as at springs.

The sandstone is typically very porous, with corrosion of quartz grains, and dissolution of kaolinite and muscovite. In the subsurface, the sandstone may be classified as a quartz arenite to sublitharenite, while epidiagenetic alterations appear to have modified the composition into a quartz arenite.

Goethite is ubiquitous in the outcrop samples, with joint faces containing anomalously high goethite abundances, and forming fracture-related groundwater ferricretes. The goethite has its iron source in pyrite and iron-bearing carbonate phases.

Mass balance calculations indicate that dissolution is the most important chemical mechanism in the outcrop. Iron is being conserved in the sandstone with the joint block interiors serving as net exporters of iron to the 1 cm thick case-hardened joint faces. All other species (Si^{4+}, Ca^{2+}, Mg^{2+}, Mn^{2+}, K^{+}, SO_4^{2-}, and Al^{3+}) are being removed in solution from the outcrop.

The ion imports/exports calculated in the mass balance model may be converted into water chemistry concentrations and compared with the modern day water chemistry of shallow Pennsylvanian aquifers. The results indicate that quartz, all carbonate phases, and pyrite are currently weathering in the shallow aquifers. The fact that K-feldspar is stable in outcrop explains why the K^{+} concentrations of the aquifers are higher than those calculated from the mass balance model. A higher concentration of Mn^{2+} in the outcrop calculations of water chemistry indicate that the only manganese-bearing phase (siderite) is being dissolved early in the aquifers, and that the aquifers may be either presently flushed of Mn^{2+}, or possibly the manganese has been exported from the joint block interiors to the joint face, much as iron is doing. Aluminum, too, has a higher concentration in reconstructed losses from

outcrop relative to the aquifer. This may be explained by the observation that all Al^{3+}-bearing phases in the subsurface are stable, while unstable in outcrop.

In terms of being a modern day unconformity surface, the Eaton sandstone exhibits the typical porosity enhancement. What is different, however, is that kaolinite is not forming as a weathering product, and diagenetic kaolinite presently is undergoing dissolution.

Unfortunately this study is unable to shed new light on the formation of honeycomb weathering.

CONCLUSIONS

(1) Outcrop mineral-water interactions are responsible for the silica saturation observed in the Pennsylvanian aquifers of the Michigan basin.

(2) Quartz dissolution was the result of goethite precipitation at the onset of weathering, but today is simply the result of quartz dissolving in undersaturated meteoric water.

(3) Muscovite is undergoing weathering to vermiculite, as well as being dissolved.

(4) Mass balance calculations indicate that the Eaton sandstone is behaving as a closed system with respect to iron, yet aluminum, as well as silica, calcium, magnesium, manganese, potassium, and sulfate, are all mobile.

(5) Pyrite oxidation alone is not responsible for creating the acidic conditions which dissolved the carbonate cement.

(6) All kaolinite in the outcrop is a diagenetic clay and is not the result of feldspar weathering. K-feldspar appears stable in outcrop.

(7) Kaolinite in outcrop is undergoing dissolution, thus implying that kaolinization of aluminosilicates below unconformity surfaces is not as important a factor in reservoir quality as was once believed.

(8) Epidiagenetic alterations appear to have modified the composition of the sandstone from a sublitharenite/quartz arenite in the subsurface to a predominantly quartz arenite in outcrop.

APPENDICES

APPENDIX A

APPENDIX A

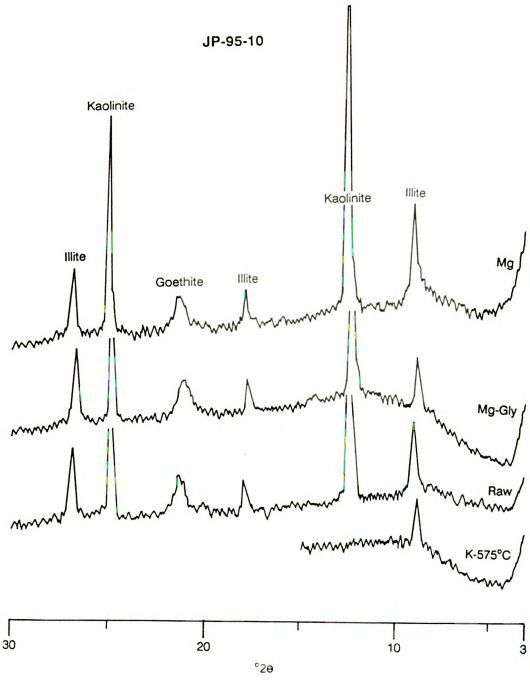

Figure 17. (a) Selected diffractograms. Sample JP-95-10

APPENDIX A (cont'd)

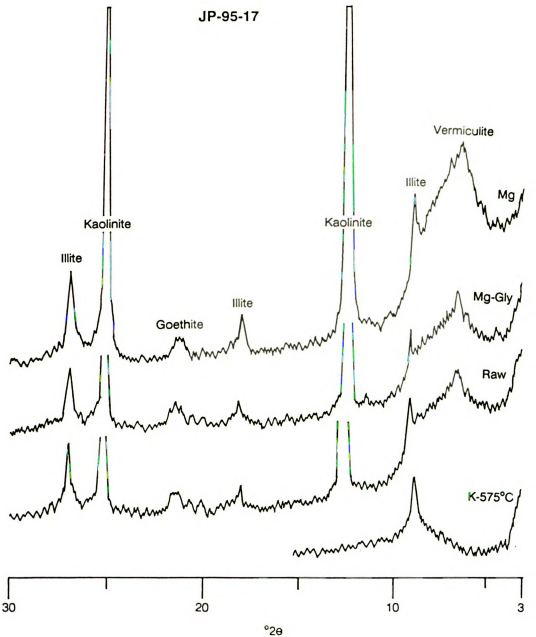

Figure 17. (b) Selected diffractograms. Sample JP-95-17

APPENDIX B

APPENDIX B

Table 15. Sample collection data.

Outcrop	Samples	Joint Plane	Sample Surface	Trend of Sample Line	Height From Base	Distance from Joint Face
2	JP-95-1	N50E,	West	N8W	6'6"	JOINT-1½"
	JP-95-2	88SE				1½-4"
	JP-95-3					4-6½"
	JP-95-4					6½-8½"
	JP-95-5					8½-11½"
	JP-95-6					11½-15"
3	JP-95-7	N53W,	Southeast	N65W	5'6"	JOINT-2"
	JP-95-8	84NE				2-4"
	JP-95-9					4-6½"
	JP-95-10					6½-8½"
	JP-95-11					8½-11"
4	JP-95-12	N40W,	North	N80W	5'0"	JOINT-2"
	JP-95-13	87SE				2"-4¼"
	JP-95-14					4¼-6¼"
	JP-95-15					6¼-8½"
6	JP-95-16	N55E,	Southwest	N55W	7'0"	JOINT-2½
	JP-95-17	90SE				2½-5"
	JP-95-18					5-7"
	JP-95-19					7-9½"
	JP-95-20					9½-12"
	JP-95-21					12-14"

APPENDIX C

APPENDIX C

Figure 18. (a) Photo of outcrop sampling. Outcrop #2

APPENDIX C (cont'd)

Figure 18. (b) Photo of outcrop sampling. Outcrop #3

APPENDIX C (cont'd)

Figure 18. (c) Photo of outcrop sampling. Outcrop #4

APPENDIX C (cont'd)

Figure 18. (d) Photo of outcrop sampling. Outcrop #6.

APPENDIX D

APPENDIX D

Clay Mineral Preparation and Identification

Preparation Techniques

Clay mineral mounts were prepared for x-ray diffraction (XRD) by a method described by Keller et al. (1986). Samples were mechanically disaggregated with mortar and pestle, and then dispersed by ultrasonification in distilled water. Separation into the clay size fraction was performed by gravity settling. The <2μm particle size fraction was separated with a pipette, and the aliquots were then filtered onto a 0.45μm Millipore filter and rinsed with distilled water, the suspensions being drawn through the filter with a vacuum. The filter cakes were transferred to standard petrographic glass slides, placed sample-side down, and "rolled" onto the glass using a glass stirring rod. The filter paper was then pealed off, leaving the ion-saturated clay cake adhering to the glass slide. Four oriented mounts of each sample were prepared; one saturated with potassium, one saturated with magnesium, one saturated with magnesium and glycolated at room temperature, and one with only the naturally-occurring exchange ions ("raw").

Clay Mineral Identification

Identification of clays follows the procedure outlined in Eslinger and Pevear (1988). Illite was identified by sharp peaks near 10 Å, 5 Å, and 3.33 Å. Identification of kaolinite

was based on two sharp peaks near 7.2 Å and 3.6 Å. Goethite was identified by a single, weak broad peak near 4.18 Å.

2:1 clay identification required a comparison of all four preparations of each individual sample, as well as heating to 575° C. Identification of vermiculite relied on the expansion from 10 Å to 14 Å when magnesium was added to the sample preparation. Its failure to expand to 17 Å when glycolated distinguished it from smectite. The absence of any 14 Å or 7 Å peaks after heating to 575° C, confirmed the lack of any chlorite in the sample.

BIBLIOGRAPHY

BIBLIOGRAPHY

Adams, W.A., and J.K. Kassim, 1983. The Origin of Vermiculite in Soils Developed from Lower Palaeozoic Sedimentary Rocks in Mid-Wales: Soil Science Society of America Journal, v. 47, pp. 316-320.

Al-Gailani, M.B., 1981. Authigenic Mineralizations at Unconformities: Implications for Reservoir Characteristics: Sedimentary Geology, v. 29, pp. 89-115.

Arditto, P.A., 1983. Mineral-Groundwater Interactions and the formation of Authigenic Kaolinite Within the Southeastern Intake Beds of the Great Australian (Artesian) Basin, New South Wales, Australia: Sedimentary Geology, v. 35, pp. 249-261.

Arnold, G.E., 1978. A Petrographic Study of Sandstone Weathering: Unpublished M.S. Thesis, West Virginia University, 54 pp.

Bennett, P.C., and D.I. Siegel, 1987. Increased Solubility of Quartz in Water due to Complexing by Organic Compounds: Nature, v. 326, no. 6114, pp. 684-686.

Bennett, P.C., Melcer, M.E., Siegel, D.I., and J.P. Hassett, 1988. The Dissolution of Quartz in Dilute Aqueous Solutions of Organic Acids at 25° C: Geochimica et Cosmochimica Acta, v. 52, pp. 1521-1530.

Bennett, P.C., Siegel, D.I., Hill, B.M., and P.H. Glaser, 1991. Fate of Silicate Minerals in a Peat Bog: Geology, v. 19, pp. 328-331.

Bjorkum, P.A., and N. Gjelsvik, 1988. An Isochemical Model for Formation of Authigenic Kaolinite, K-Feldspar, and Illite in Sediments: Journal of Sedimentary Petrology, v. 58, no. 3, pp. 506-511.

Bjorkum, P.A., Mjos, R., Walderhaug, O., and A. Hurst, 1990. The Role of the Late Cimmerian Unconformity for the Distribution of Kaolinite in the Gullfaks Field, North Sea: Sedimentology, v. 37, pp. 395-406.

Bjorlykke, K., 1984. Formation of Secondary Porosity. How Important is it?: In McDonald, D.A. and R.C. Surdam (eds.), Clastic Diagenesis, American Association of Petroleum Geologists Memoir 37, pp. 277-286.

Bromley, M., 1992. Topographic Inversion of Early Interdune Deposits, Navajo Sandstone (Lower Jurassic), Colorado Plateau, U.S.A.: Sedimentary Geology, v. 80, pp. 1-25.

Busenberg, E., and D.V. Clemency, 1976. The Dissolution Kinetics of Feldspars at 25° C and 1 atm CO_2 Partial Pressure: Geochimica et Cosmochimica Acta, v. 40, pp. 41-50.

Butler, P.R., and J.F. Mount, 1986. Corroded Cobbles in Southern Death Valley: Their Relationship to Honeycomb Weathering and Lake Shorelines: Earth Surface Processes and Landforms, v. 11, pp. 377-387.

Campbell, I.A., 1991. Classification of Rock Weathering at Writing-on-Stone Provincial Park, Alberta, Canada: A Study in Applied Geomorphology: Earth Surface Processes and Landforms, v. 16, pp. 701-711.

Chigira, M., and K. Sone, 1991. Chemical Weathering Mechanisms and Their Effects on Engineering Properties of Soft Sandstone and Conglomerate Cemented by Zeolite in a Mountainous Area: Engineering Geology, v. 30, pp. 195-219.

Chittleborough, D.J., 1989. Genesis of a Xeralf on Feldspathic Sandstones, South Australia: Journal of Soil Science, v. 40, pp. 235-250.

Cohee, G.V., 1965. Geologic History of the Michigan Basin: Journal of the Washington Academy of Sciences, v. 55, pp. 211-224.

Dannemiller, G.T., and M.A. Baltusis, 1990. Physical and Chemical Data for Ground Water in the Michigan Basin, 1986-1989: U.S. Geological Survey Open-File Report 90-368, 155 pp.

Davis, M.W., and H.D. Bredwell, 1978. Geology; in The Nature of Grand Ledge; Grand Ledge Area American Revolution Bicentennial Commission, pp. 7-37.

Drever, J.I., 1988. The Geochemistry of Natural Waters: Prentice Hall, Inc., Englewood Cliffs, 437 pp.

Emery, D., Myers, K.J., and R. Young, 1990. Ancient Subaerial Exposure and Freshwater Leaching in Sandstones: Geology, v. 18, pp. 1178-1181.

Eslinger, E., and D. Pevear, 1988. Clay Minerals for Petroleum Geologists and Engineers: SEPM Short Course Notes no. 22, 413 pp.

Fairbridge, R.W., 1967. Phases of Diagenesis and Authigenesis: In G. Larsen and G.V. Chilinger (eds.), Diagenesis in Sediments, Elsevier, Amsterdam, pp. 19-89.

Ganesh, A., and S. Sathyanarayan, 1991. Origin of Miniature Pits in the Quartz-Arenites of the Badami Group (Younger Proterozoic), Umatar, Belgaum District, Karnataka: Journal if the Geological Society of India, v. 38, pp. 621-624.

Gill, E.D., Segnitt, E.R., and N.H. McNeill, 1981. Rate of Formation of Honeycomb Weathering Features (Small Scale Tafoni) on the Otway Coast, S.E. Australia: Proceedings of the Royal Society of Victoria, v. 92, pp. 149-154.

Goudie, A., 1973. Duricrusts in Tropical and Subtropical Landscapes: Clarendon Press, Oxford, 174 pp.

Heald, M.T., Hollingsworth, T.J., and R.M. Smith, 1979. Alteration of Sandstone as Revealed by Spheroidal Weathering: Journal of Sedimentary Petrology, v. 49, pp. 901-910.

Hollingsworth, T.J., 1977. Spheroidal Weathering of Sandstones in Nicholas County, West Virginia: Unpublished M.S. Thesis, West Virginia University, 84 pp.

Hudson, R.J., 1957. Genesis and Depositional History of the Eaton Sandstone, Grand Ledge, Michigan: Unpublished M.S. Thesis, Michigan State University, 49 pp.

Keller, W.D., Reynolds, R.C., and A. Inoue, 1986. Morphology of Clay Minerals in the Smectite-to-Illite Conversion Series by Scanning Electron Microscopy: Clays and Clay Minerals, v. 34, no. 2, pp. 187-197.

Kelletat, D., 1980. Studies on the Age of Honeycombs and Tafoni Features: Catena, v. 7, pp. 317-325.

Kelly, W.A., 1933. Pennsylvanian Stratigraphy Near Grand Ledge, Michigan: Journal of Geology, v. 41, pp. 77-88.

----------, 1936. The Pennsylvanian System in Michigan: Michigan Geological Survey Publication 40, Geological Series 34, part 2, pp. 149-226.

Klein, C., and C.S. Hurlbut, 1985. Manual of Mineralogy: John Wiley & Sons, Toronto, 596 pp.

Kramer, R.S., and D.B. Westjohn, 1991. Textures, and Chemical and Isotopic Compositions of Authigenic Carbonates in Pennsylvanian Sandstones in the Michigan Basin: Unpublished United States Geological Survey Report, Lansing, Michigan.

Krauskopf, K.B., 1956. Dissolution and Precipitation of Silica at Low Temperatures: Geochimica et Cosmochimica Acta, v. 10, pp. 1-26.

Land, L.S., and K.L. Milliken, 1981. Feldspar Diagenesis in the Frio Formation, Brazoria County, Texas Gulf Coast: Geology, v. 9, pp. 314-318.

Lin, F., and C.V. Clemency, 1981. The Kinetics of Dissolution of Muscovite at 25° C and 1 atm CO_2 Partial Pressure: Geochimica et Cosmochimica Acta, v. 45, pp. 571-576.

Long, D.T., Wilson, T.P., Takacs, M.J., and D.H. Rezabek, 1988. Stable-Isotope Geochemistry of the Saline Near-Surface Ground Water: East Central Basin: Geological Society of America Bulletin, v. 100, pp. 1568-1577.

Long, D.T., Badulamenti, L., and T.P. Wilson, 1990. The Role of Glaciation in Controlling the Geochemical Interaction of Near Surface Groundwater and Formation Brine: Geological Society of America Abstracts with Programs, v. 22, p 31.

Martin, J.R., 1982. Pennsylvanian Deltaic Sedimentation in Grand Ledge, Michigan: Unpublished M.S. Thesis, Western Michigan University, 131 pp.

McBride, E.F., 1987. Diagenesis of the Maxon Sandstone (Early Cretaceous), Martin Region, Texas: A Diagenetic Quartz-Arenite: Journal of Sedimentary Petrology, v. 57, pp. 98-107.

McGreevy, J.P., 1985. A Preliminary Scanning Electron Microscope Study of Honeycomb Weathering of Sandstone in a Coastal Environment: Earth Surface Processes and Landforms, v. 10, pp. 508-518.

Meissner, B.D., 1993. The Geochemistry and Source for Solutes in Ground Water from the Pennsylvanian Bedrock Sequence in the Michigan Basin: Unpublished M.S. Thesis, Michigan State University, 115 pp.

Meissner, B.D., Long D.T., Wahrer, M.A., Bauer, P.N., Lee, R.W., and T.P. Wilson, 1992. Geochemistry and Source of Solutes in Ground Water from the Marshall Sandstone Regional Aquifer, Michigan Basin: Geological Society of America Abstracts with Programs, v. 24, no. 7, p. A240.

Merino, E., 1975a. Diagenesis in Tertiary Sandstones from Kettleman North Dome, California--I. Diagenetic Mineralogy: Journal of Sedimentary Petrology, v. 45, no. 1, pp. 320-336.

Merino, E., 1975b. Diagenesis in Tertiary Sandstones from Kettleman North Dome, California--II. Interstitial Solutions: Distribution of Aqueous Species at 100° C and Chemical Relation to the Diagenetic Mineralogy: Geochimica et Cosmochimica Acta, v. 39, pp. 1629-1645.

Morris, R.C., and A.B. Fletcher, 1987. Increased Solubility of Quartz Following Ferrous-Ferric Iron Reactions: Nature, v. 330, pp. 558-561.

Mustoe, G.E., 1982. The Origin of Honeycomb Weathering: Geological Society of America Bulletin, v. 93, pp. 108-115.

Mustoe, G.E., 1983. Cavernous Weathering in the Capitol Reef Desert, Utah: Earth Surface Processes and Landforms, v. 8, pp. 517-526.

Nedkvitne, T., and K. Bjorlykke, 1992. Secondary Porosity in the Brent Group (Middle Jurassic), Huldra Field, North Sea: Implications for Predicting Lateral Continuity of Sandstones?: Journal of Sedimentary Petrology, v. 62, no. 1, pp. 23-34.

Nahon, D., Carozzi, A.V., and C. Parron, 1980. Lateritic Weathering as a Mechanism for the Generation of Ferruginous Ooids: Journal of Sedimentary Petrology, v. 50, pp. 1287-1298.

Nesbitt, W.H., 1980. Characterization of Mineral-Formation Water Interactions in Carboniferous Sandstones and Shales of the Illinois Sedimentary Basin: American Journal of Science, v. 280, pp. 607-630.

Nott, J.F., Idnurn., M., and R.W. Young, 1991. Sedimentology, Weathering, Age and Geomorphological Significance of Tertiary Sediments on the Far South Coast of New South Wales: Australian Journal of Earth Sciences, v. 38, pp. 357-373.

Parron, C., and D. Nahon, 1980. Red Bed Genesis by Lateritic Weathering of Glauconitic Sediments: Journal of the Geological Society (London), v. 137, pp. 689-693.

Peters, N.E., and J.E, Bonelli, 1982. Chemical Composition of Bulk Precipitation in the North-Central and North-eastern United States, December 1980 Through February 1981: Geological Survey Circular 874, 63 pp.

Pettijohn, F.J., Potter, P.E., and R. Siever, 1987. Sand & Sandstone: Springer-Verlag, New York, 553 pp.

Rich, C.I., 1958. Muscovite Weathering in a Soil Developed in the Virginia Piedmont: In Clays and Clay Minerals, Fifth National Conference on Clays and Clay Minerals, National Academy of Sciences-National Research Council, publication 566, Ada Swineford (ed.), pp. 203-212.

Richardson, S.M., and H.Y. McSween, 1989. Geochemistry: Pathways and Processes: Prentice Hall, Englewood Cliffs, 488 pp.

Robinson, D.A., and R.B.G. Williams, 1992. Sandstone Weathering in the High Atlas, Morocco: Z. Geomorph. N.F., v. 36, no. 4, pp. 413-429.

Sancho, C., and G. Benito, 1990. Factors Controlling Tafoni Weathering in the Ebro Basin (N.E. Spain): Z. Geomorph. N.F., v. 34, no. 2, pp. 165-177.

Sancho, C., and M. Gutierrez, 1990. Analysis Morfometrico De La Tafoniza De La Arenisca De Peraltilla (Anticlinal De Barbastro, Depresion Del Ebro): Influencia De Los Factores Mineralogic-Texturales: Cuaternario y Geomorfologia, v. 4, pp. 131-145.

Shanmugam, G., 1988. Origin, Recognition and Importance of Erosional Unconformities in Sedimentary Basins: In New Perspectives in Basin Analysis, Kleinspehn, K.L. and C. Paola (eds.), Springer-Verlag, New York, pp. 83-108.

Shanmugam, G., and J.B. Higgins, 1988. Porosity Enhancement from Chert Dissolution Beneath Neocomian Unconformity, Ivishuk Formation, North Slope, Alaska: American Association of Petroleum Geologists Bulletin, v. 72, pp. 523-535.

Shanmugam, G., 1990. Porosity Prediction in Sandstones Using Erosional Unconformities: In Prediction of Reservoir Quality Through Chemical Modeling, Meshri, I.D. and P.J. Ortoleva (eds.), American Association Petroleum Geologists Memoir 49, pp. 1-23.

Siever, R., 1962. Silica Solubility, 0-200° C and the Diagenesis of Siliceous Sediments: Journal of Geology, v. 70, pp. 127-150.

Singh, R.N., Grube, W.E., Jr., Smith, R.M., and R.F. Keefer, 1982. Relation of Pyritic Sandstone Weathering to Soil and Minesoil Properties: In Acid Sulfate Weathering, Kittrick, J.A., Fanning, D.S., Hossner, L.R., Kral, D.M. and S. Hawkins (eds.), Soil Science Society of America Special Publication Number 10, pp. 193-207.

Smith, P.J., 1982. Why Honeycomb Weathering?: Nature, v. 298, pp. 121-122.

Smith, P.J., 1983. Can Honeycomb Weathering be ET?: Nature, v. 301, p.291.

State of Michigan, 1966. Laws Relating to Water: A Comprehensive Planning Study of the Grand River Basin, Michigan: Lansing, Michigan, 415 pp.

Stearns, M.D., 1933. The Petrology of the Marshall Formation of Michigan: Journal of Sedimentary Petrology. v. 3, pp. 99-112.

Summerfield, M.A., 1983. Silcrete: In Chemical Sediments and Geomorphology, Goudie, A.S., and K. Pye (eds.), Academic Press, London, pp. 59-91.

Tardy, Y., 1971. Characterization of the Principal Weathering Types by the Geochemistry of Waters from some European and African Crystalline Massifs: Chemical Geology, v. 7, pp. 253-271.

Thiry, M., Ayrault, M.B., and J.C. Grisoni, 1988. Ground-Water Silicification and Leaching in Sands: Example of the Fontainebleau Sand (Oligocene) in the Paris Basin: Geological Society of America Bulletin, v. 100, pp. 1283-1290.

Thiry, M., and A.R. Milnes, 1991. Pedogenic and Groundwater Silcretes at Stuart Opal Field, South Australia: Journal of Sedimentary Petrology, v. 61, pp. 111-127.

Velbel, M.A., and D.S. Brandt, 1989. Sedimentology and Paleography of the Pennsylvanian Strata of Grand Ledge, Michigan: Michigan Basin Geological Society Field Trip Guidebook, 33 pp.

Velbel, M.A., and J. Genuise, 1988. Clay Minerals in Underclays and Other Kaolinitic Mudrocks of the Saginaw Formation and Eaton Sandstone (Pennsylvanian Grand River Group), Grand Ledge, Michigan: Abst., 1988 Annual Meeting, Clay Minerals Society, p. 35.

Vicente, M.A., 1983. Clay Mineralogy as the Key Factor in Weathering of "Arenisca Dorada" (Golden Sandstone) of Salamanca, Spain: Clay Minerals, v. 18, pp. 215-217.

Wahrer, M.A., 1993. The Geochemistry and Source of Solutes in Ground Water from the Glacial Drift Regional Aquifer, Michigan Basin: Unpublished M.S. Thesis, Michigan State University, 111 pp.

Wahrer, M.A., Long, D.T., Meissner, B.D., and D.B. Westjohn, 1992. Geochemistry and Source of Solutes in Ground Water from Near-Surface-Bedrock and Glacial-Drift Regional Aquifers, Michigan Basin: Geological Society of America Abstracts with Programs, v. 24, no. 7, p. A240.

Wallis, J.L., and M.A. Velbel, 1985. Honeycomb Weathering of Pennsylvanian Sandstones, Grand Ledge, Michigan: Geological Society of America Abstracts with Programs, v. 17, p. 330.

Weed, R., and R.P. Ackert Jr., 1986. Chemical Weathering of Beacon Supergroup Sandstones and Implications for Antarctic Glacial Chronology: South African Journal of Science, v. 82, pp. 513-516.

Westjohn, D.B., H.W. Olsen, and A.T. Willden, 1990. Matrix-Controlled Hydraulic Properties of Mississippian and Pennsylvanian Sandstones from the Michigan Basin: U.S. Geological Survey Open-File Report 90-104, 18 pp.

Westjohn, D.B., and D.F. Sibley, 1991. Geophysical and Hydraulic Properties of Mississippian Sandstones from the Michigan Basin, and Their Relations to Mineralogy and Stratigraphy: Geological Society of America Abstracts with Programs, v. 23, p 26.

Westjohn, D.B., Sibley, D.F., and J.A. Eluskie, 1991. Authigenic Mineral Paragenesis in Mississippian and Pennsylvanian Sandstone Aquifers in the Michigan Basin: Geological Society of America Abstracts with Programs, v. 23, p. 327.

White, J.L., 1962. X-Ray Diffraction Studies on the Weathering of Muscovite: Soil Science, v. 93, no. 1, pp. 16-21.

Williams, R., and D. Robinson, 1989. Origin and Distribution of Polygonal Cracking of Rock Surfaces: Geografiska Annaler, v. 71A, pp. 145-159.

Wilson, M.D., and E.D. Pittman, 1977. Authigenic Clays in Sandstones: Recognition and Influence on Reservoir Properties and Palaeo-Environmental Analysis: Journal of Sedimentary Petrology, v. 47, pp. 3-31.

Wood, W.W., 1969. Geochemistry of Ground Water of the Saginaw Formation in the Upper Grand River Basin, Michigan: Unpublished Ph.D. Thesis, Michigan State University, 104 pp.

Young, R.W., 1986. Tower Karst in Sandstone: Bungle Bungle Massif, Northwestern Australia: Z. Geomorph. N.F., v. 30, no. 2, pp. 189-202.

Young, R.W., 1987. Sandstone Landforms of the Tropical East Kimberley Region, Northwestern Australia: Journal of Geology, v. 95, pp. 205-218.

Young, R.W., 1988. Quartz Etching and Sandstone Karst: Example from the East Kimberleys, Northwestern Australia: Z. Geomorph N.F., v. 32, no. 4, pp. 409-423.

Young R.W., and R.M. Young, 1988. "Altogether Barren, Peculiarly Romantic": The Sandstone Lands Around Sydney: Australian Geographer, v. 19, no. 1, pp. 9-25.

Young R.W., and A. Young, 1992. Sandstone Landforms: Springer-Verlag, New York, 163 pp.

Zacharias, K.F., 1992. Clay Mineral Diagenesis in the Marshall Sandstone, Michigan Basin: Unpublished M.S. Thesis, Michigan State University, 95 pp.

Zacharias, K.F., Sibley, D.F., and D.T. Long, 1992. Detrital Diagenesis, Hydraulic Conductivity and Pore Water Chemistry in the Marshall Sandstone Regional Aquifer, Michigan Basin: Geological Society of America Abstracts with Programs, v. 24, no. 7, p. A240.